Chinese Journal of
POLYMER SCIENCE

FEATURE ARTICLE

• 2026 Rising Scholars •

https://doi.org/10.1007/s10118-026-3621-x
Chinese J. Polym. Sci. **2026**, *44*, 2062–2085

Recent Advances in Nickel- and Palladium-catalyzed Copolymerization of Ethylene with Fundamental Polar Monomers

Kang-Kang Li and Zhong-Bao Jian*

State Key Laboratory of Polymer Science and Technology, Changchun Institute of Applied Chemistry, Chinese Academy of Sciences, Changchun 130022, China

Abstract Coordination-insertion copolymerization of ethylene with polar vinyl monomers offers a direct route to functionalized polyolefins, enabling regular incorporation of polar groups under mild conditions and superior microstructural control compared with post-functionalization or radical routes. The persistent polar monomer problem—the tendency of polar groups to coordinate to or poison active metal sites—motivates the focus on late-transition-metal catalysts, chiefly Ni and Pd. Recent advances in ligand design, catalyst engineering, and monomer modification have improved comonomer incorporation, suppressed chain transfer, and enhanced thermal robustness. Mechanistic studies now resolve 2,1- versus 1,2-insertion, ligand-induced chelate isomerization, and polar-monomer-promoted chain-transfer pathways. This feature article surveys nickel- and palladium-based catalytic systems reported from 2020 onward for copolymerization of ethylene with fundamental polar monomers, with an emphasis on acrylates, while also covering acrylic acid, vinyl acetate, butyl vinyl ether, acrylonitrile, acrylamide, vinyl silyl ethers, and selected disubstituted monomers, categorizing recent advances by key ligand classes ([N,N], [N,O], [P,O]) and linking mechanism, selectivity, and polymer properties to guide catalyst design and scale-up.

Keywords Nickel and palladium catalysts; Polar monomers; Coordination-insertion polymerization; Polyolefin

Citation: Li, K. K.; Jian, Z. B. Recent advances in nickel- and palladium-catalyzed copolymerization of ethylene with fundamental polar monomers. *Chinese J. Polym. Sci.* **2026**, *44*, 2062–2085.

* Corresponding author, E-mail: zbjian@ciac.ac.cn
Received January 14, 2026; Accepted February 9, 2026; Published online April 30, 2026

1 INTRODUCTION

Polyolefins, and polyethylene in particular, underpin the modern industry owing to their abundant feedstock and scalable processing.[1,2] The global polyolefin market is projected to exceed USD 200 billion by 2024 and expand at an average annual growth rate of approximately 5.4% by 2030.[3] The hydrocarbon backbone of polyethylene confers chemical resistance and processing robustness, while tunable crystallinity, melting point, and mechanical properties enable applications ranging from commodity packaging to engineered parts.[4–6] The same nonpolar backbone limits the surface wettability, interfacial adhesion, dyeability, and compatibility with polar substrates—shortcomings that constrain multiphase designs and high-performance interfaces.[7–9] Traditional approaches to functionalized polyolefins—post-polymerization modification, radical copolymerization, and olefin metathesis-derived pathways—retain value but suffer intrinsic drawbacks. Post-modification often induces chain scission, crosslinking, and poorly defined microstructures.[10–12] Alternatively, the conventional high-pressure radical copolymerization of ethylene with polar comonomers requires extreme conditions and yields broad, highly branched products. Controlled radical methods, such as reversible addition-fragmentation chain transfer polymerization (RAFT), atom transfer radical polymerization (ATRP), and nitroxide-mediated polymerization (NMP), improve structure control; however, their applications in direct ethylene/polar comonomer copolymerization are hampered by the instabil-

ity of the propagating ethylene radical and the high energetic barrier for reversibly activating the dormant chain end.[13,14] Additionally, olefin metathesis routes are limited by restricted monomer availability, high catalyst costs, and challenges in removing residual metals from the polymer product.[15]

In contrast, coordination-insertion copolymerization of ethylene with polar monomers, mediated by well-defined transition-metal complexes, offers a direct route to incorporate polar functionality under milder conditions with superior microstructural control.[16–19] The central obstacle, the polar monomer problem, lies in the strong coordination or poisoning of metal active sites by polar groups, which promotes β-H elimination, chain transfer, and catalyst deactivation.[20] The Ziegler-Natta and metallocene systems, primarily based on early transition metals (*e.g.*, Ti and Zr), are typically hard Lewis acids with high oxophilicity. Consequently, Lewis basic polar monomers tend to coordinate strongly to these electrophilic metal centers, blocking ethylene coordination, and leading to irreversible catalyst poisoning.[21–25] By contrast, late transition metals, notably nickel and palladium, are softer Lewis acids with intrinsically reduced oxophilicity, so metal–heteroatom interactions are weaker and more reversible. This fundamental electronic distinction renders Ni and Pd catalysts significantly more tolerant to polar functional groups. When paired with judiciously designed ligands (*e.g.*, bulky α-diimine or phosphine-sulfonate), these Ni/Pd systems can further destabilize dormant metal-chelate resting states, thereby facilitating continuous chain growth. Crucially, the inherent capacity of these Ni/Pd catalysts to undergo chain walking and tolerate impurities makes them particularly promising candidates for the direct synthesis of functionalized polyolefins with tunable microstructures.[26–30] Ideally illustrating this structural versatility, Brookhart's bulky cationic α-diimine Ni/Pd complexes pioneered chain-walking routes to highly branched, ester-functionalized polyethylene,[31–40] while Drent's phosphine-sulfonate Pd platforms demonstrated access to linear functionalized polyethylene.[41–48] Building on these foundations, recent ligand engineering of phosphine-phenolate Ni systems—introducing enhanced steric bulk and electronic tuning—has materially improved activity and molecular weight (MW) control, renewing momentum in the field.[49–52]

Focusing on the advances reported since 2020, this feature article examines nickel- and palladium-based systems for the copolymerization of ethylene with fundamental polar monomers, emphasizing acrylates while also encompassing acrylic acid, vinyl acetate, butyl vinyl ether, acrylonitrile, acrylamide, vinyl silyl ethers, and selected disubstituted monomers (Fig. 1). Progress is organized according to major ligand classes ([N,N], [N,O], and [P,O]), with correlations drawn between mechanistic features, insertion selectivity, and polymer microstructure to inform rational catalyst design and assess their potential for future scale-up. Particular emphasis is placed on the thermal robustness for industrial solution polymerization and heterogenization strategies to prevent reactor fouling, bridging the gap between academic research and industrial implementation.

2 NICKEL CATALYSTS

The abundance and low cost of nickel have driven sustained efforts to develop high-performance Ni catalysts for coordination-insertion copolymerization. Early Ni systems were largely restricted to a narrow set of polar-modified norbornene derivatives and a few ω-functionalized olefins.[53,54] Progress in ligand design and catalyst architecture has broadened the comonomer scope of Ni catalysts to include fundamental polar monomers such as acrylates, with marked gains in activity and MW control.[55–57] Nevertheless, relative to palladium, the nickel center exhibits higher oxophilicity, rendering the efficient copolymerization of ethylene with acrylates particularly challenging. Recent work can be grouped into several ligand families—bidentate [N,N], [N,O], and [P,O] frameworks, as well as other tailored Ni complexes—and focuses on two complementary strategies.[17,58,59] One strategy increases local steric shielding and tunes electronic donation to suppress undesired chain transfer and β-H elimination, thereby raising the polymer MW. The other employs constrained or dynamic architectures to improve tolerance toward polar comonomers and promote insertion. The following sections examine representative implementations of these strategies, summarize the performance metrics in ethylene copolymerization with fundamental polar monomers, and provide mechanistic insights that inform next-generation Ni catalyst design.

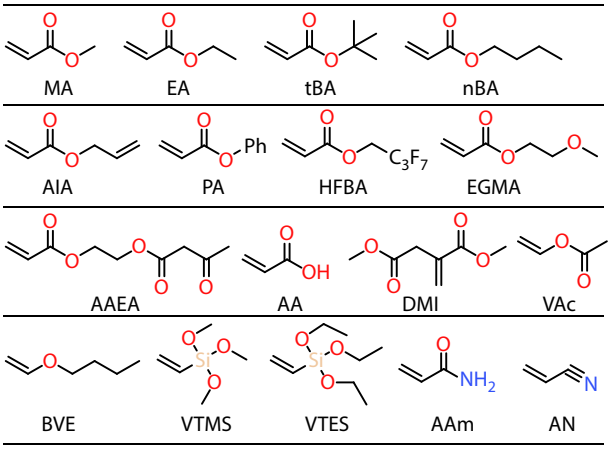

Fig. 1 Chemical structures of representative polar monomers.

2.1 [N,N] Ni Catalysts

2.1.1 α-Diimine Ni catalysts

Conventional α-diimine Ni catalysts are typically inactive for ethylene/methyl acrylate (MA) copolymerization under mild conditions, historically requiring harsh conditions for polar incorporation.[56] However, precise ligand design, targeting steric environments and secondary interactions, has recently overcome these limitations.[60,61]

Gao *et al.* exploited noncovalent Ni-phenyl contacts in "sandwich" dibenzobarrelene-derived α-diimine nickel catalysts **1** bearing 8-(*p*-substituted-phenyl)naphthyl substituents to enable the direct copolymerization of ethylene with MA (Fig. 2).[62] Catalytic performance correlated with the strength of noncovalent Ni–phenyl interactions (Me > OMe > CF_3) rather than the simple electron-donating capability of the substituents (OMe > Me > CF_3), and the Me variant **1b** delivered an activity of 6.9×10^3 g·mol^{-1}·h^{-1} to yield lightly branched poly(ethylene-*co*-methyl acrylate) (EMA) (incorporation: 2.1 mol%; 44 brs/1000C) at 1.0 mol·L^{-1} MA, while re-

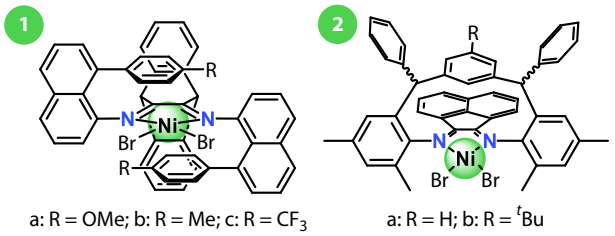

Fig. 2 *α*-Diimine Ni catalysts.

taining activity (4.5×10^3 g·mol^{-1}·h^{-1}) and increasing MA incorporation to 5.2 mol% at 100 °C. DFT calculations indicated that the Ni-aryl contact destabilized the MA *σ*-complex, lowered $\Delta\Delta G$ for conversion to the active *π*-complex, and enabled 2,1-insertion followed by ethylene insertion with little chelate-size bias, producing polymers containing internal, side-chain, and terminal MA units akin to radical EMA.

Distinct from traditional strategies for constructing axial shielding—such as utilizing sandwich-type arylamines or introducing bulky steric hindrance at the ortho-positions of arylamines—Liu *et al.* implemented an "occupancy" strategy in macrocyclic *α*-diimine Ni(II) catalysts **2** by introducing axial anagostic Ni···H—C contacts that sterically and electronically block axial approach and suppress associative chain transfer (Fig. 2); *meso*-(S,R)-**2a**, though moderately active (1.3×10^5–2.9×10^5 g·mol^{-1}·h^{-1}), afforded ultra-high molecular weight (UHMW) copolymer (M_w=927 kg·mol^{-1}) with MA incorporation of 0.67 mol%.[63] Crystallography and DFT showed that the axial anagostic H···Ni interaction impeded the monomer approach and stabilized the active site *via* persistent weak interactions, maintaining a pseudo-14-electron state that suppressed chain transfer without requiring ligand dissociation.

2.1.2 Pyridine-imine Ni catalysts

Pellecchia *et al.* systematically correlated pyridine-C6 substituents with iminopyridyl Ni copolymerization performance (Fig. 3).[64] The highly hindered **3a** exhibited the highest activity (1.5×10^4 g·mol^{-1}·h^{-1}) and low M_n (4.5 kg·mol^{-1}) but minimal MA incorporation (0.5 mol%), whereas the less hindered **3c**—although less active—produced highly branched, low-M_n oil with MA up to 35 mol% (M_n=0.3 kg·mol^{-1}). Additionally, the investigation demonstrated that the activation protocol and solvent strongly influenced *β*-H elimination and chain walking, thereby dictating the in-chain versus terminal placement of MA units. Extending this theme, Pellecchia *et al.* incorporated dibenzocycloheptyl groups into the iminopyridyl skeleton to curb the formation of oily products and successfully synthesized solid, semi-crystalline EMA copolymers.[65] Structure-property analysis revealed that ethyl variant **4b** favored high activity and in-chain insertion (1.0 mol% MA; M_n: 3.3 kg·mol^{-1}), bulkier isopropyl analog **4c** lowered activity, but increased M_n (4.0 kg·mol^{-1}) and incorporation (2.0 mol%) with mixed insertion patterns (in-chain and end-of-chain MA incorporation), while electron-withdrawing halogens (**4d** and **4e**) maximized MA uptake (up to 2.5 mol%) at the cost of activity.

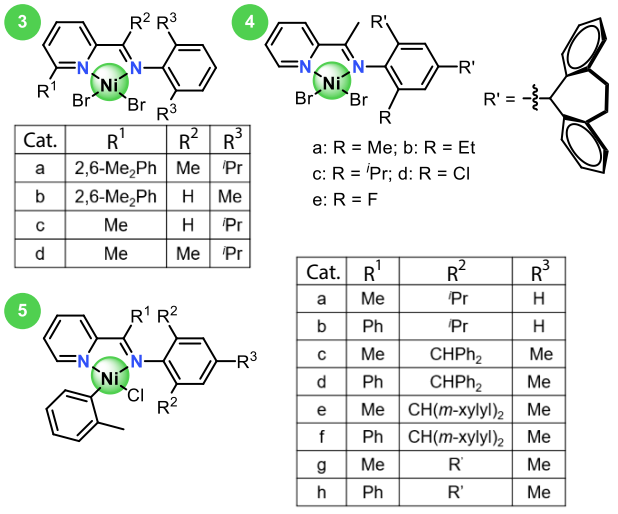

Cat.	R^1	R^2	R^3
a	2,6-Me$_2$Ph	Me	^{i}Pr
b	2,6-Me$_2$Ph	H	Me
c	Me	H	^{i}Pr
d	Me	Me	^{i}Pr

Cat.	R^1	R^2	R^3
a	Me	^{i}Pr	H
b	Ph	^{i}Pr	H
c	Me	$CHPh_2$	Me
d	Ph	$CHPh_2$	Me
e	Me	CH(*m*-xylyl)$_2$	Me
f	Ph	CH(*m*-xylyl)$_2$	Me
g	Me	R'	Me
h	Ph	R'	Me

Fig. 3 Pyridine-imine Ni catalysts.

To avoid the limitations of alkyl-aluminum activation, Harth *et al.* developed air-stable alkylated iminopyridyl Ni precursors **5,** which were activated by borane-halide abstraction to generate well-defined cationic centers with inner-sphere $ClB(C_6F_5)_3^-$ pairing (Fig. 3).[66] The combination of tight ion pairing and sterically demanding dibenzocycloheptyl substituents, which impose a significant rotational barrier, effectively suppresses chain transfer pathways. Consequently, the bulky catalyst **5g** afforded high-molecular-weight EMA (M_n=35.8 kg·mol^{-1}; incorporation: 2.2 mol%) with moderate activity (3.8×10^3 g·mol^{-1}·h^{-1}), while also successfully incorporating vinyltriethoxysilane (5.9 mol%) and vinyl acetate (0.26 mol%), respectively. Computational studies revealed that this inner-sphere pairing modulated dormant states, facilitating microstructure control without compromising activity.

2.2 [N,O] Ni Catalysts

Following Grubbs' seminal introduction of neutral salicylaldiminato [N,O] Ni catalysts, continuous structural modulation has been pursued, with studies revealing that these systems inherently undergo chain walking to yield branched microstructures.[53,54,67,68] However, the efficient incorporation of fundamental polar monomers (*e.g.*, acrylates) using salicylaldiminato Ni catalysts remains challenging, primarily because of the competitive coordination of Lewis basic functionalities that form stable chelates, which hinder olefin insertion and facilitate *β*-H elimination.[26] Consequently, improved frameworks employing cationic precursors, bimetallic architectures, or enhanced steric/electronic shielding have been developed to mitigate these limitations, as illustrated by the representative variants in Figs. 4–6.

Chen *et al.* introduced a cationic *α*-imino-ketone Ni platform that combines synthetic simplicity with pronounced monomer selectivity (Fig. 4).[69] For ethylene/MA copolymerization, catalyst **6** exhibited modest performance, giving MA incorporation up to 0.6 mol%, together with a moderate copolymerization activity of 2.5×10^3 g·mol^{-1}·h^{-1} and an M_n of 17.9 kg·mol^{-1}. In contrast, the same scaffold proved highly permissive toward siloxane comonomers: copolymerization of ethylene with vinyltrimethoxysilane (VTMS) yielded an activity of 2.2×10^5 g·mol^{-1}·h^{-1} with incorporation reaching 10.8 mol%, demonstrating that the open spatial framework selectively accommodates silicon-containing monomers. Building on this motif, Jian *et al.* introduced an "*ortho*-F" modification to mitigate carbonyl coordination.[70] The parent non-fluorinated catalyst (**7a**) was fully deactivated in ethylene/MA

https://doi.org/10.1007/s10118-026-3621-x

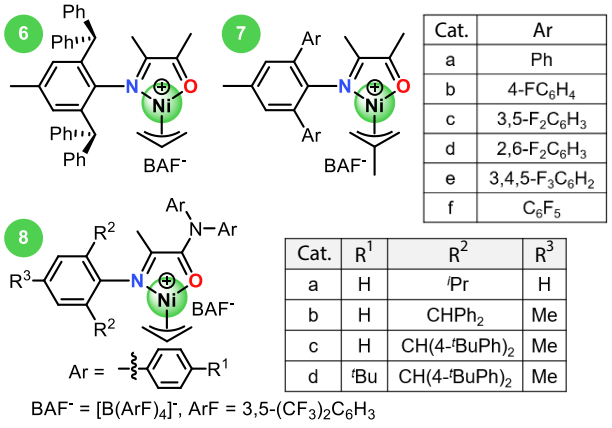

Cat.	Ar
a	Ph
b	4-FC_6H_4
c	3,5-$F_2C_6H_3$
d	2,6-$F_2C_6H_3$
e	3,4,5-$F_3C_6H_2$
f	C_6F_5

Cat.	R^1	R^2	R^3
a	H	^{i}Pr	H
b	H	$CHPh_2$	Me
c	H	CH(4-^{t}BuPh)$_2$	Me
d	^{t}Bu	CH(4-^{t}BuPh)$_2$	Me

Fig. 4 *α*-Imino-ketone Ni catalysts.

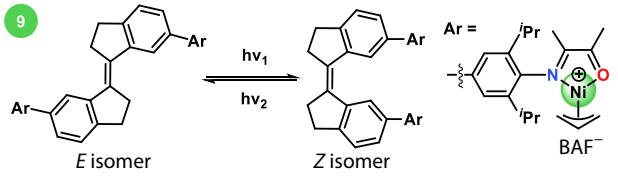

Fig. 5 Dinuclear [N,O] Ni catalysts.

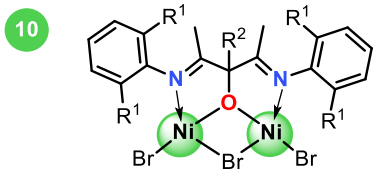

Cat.	R^1	R^2
a	Me	Me
b	^{i}Pr	Me
c	^{i}Pr	Et

Fig. 6 Dinuclear [N,O] Ni catalysts.

copolymerization because of strong ketone-Ni binding. By contrast, introduction of *ortho*-difluoro substitution (**7d**) restored MA tolerance, affording an activity of *ca.* 5.0×10^3 g·mol^{-1}·h^{-1} and yielding EMA with an M_w of 6.0 kg·mol^{-1} and 0.9 mol% incorporation, suggesting that proximal F provide a competitive weak coordination interaction (Ni···F) with the metal center that competes with the carbonyl group to suppress deleterious chelation.

To overcome the temperature limitations (20–80 °C) of previous systems, Wang *et al.* incorporated bulky diphenylamino substituents into the *α*-imino-ketone scaffold, enhancing thermal stability up to 150 °C (Fig. 4).[71] In ethylene/MA copolymerization at 110 °C, the bulky catalyst **8d** surpassed the less hindered **8a**, delivering superior activity (1.3×10^5 g·mol^{-1}·h^{-1} versus 2.5×10^4 g·mol^{-1}·h^{-1}) and M_n (1.5×10^5 g·mol^{-1} versus 1.6×10^4 g·mol^{-1}). Catalyst **8d** also maintained high activity, and M_n with *n*-butyl acrylate (*n*BA) and heptafluorobutyl acrylate (HFBA) (*n*BA: 1.3×10^5 g·mol^{-1}·h^{-1}; HFBA: 4.3×10^4 g·mol^{-1}·h^{-1}; both yielding M_n>100 kg·mol^{-1}), but the performance dropped sharply with highly hindered phenyl acrylate (PA), which gave low activity (2.2×10^4 g·mol^{-1}·h^{-1}), low incorporation (0.5 mol%), and lower M_n (47 kg·mol^{-1}). Notably, the bulky catalyst **8d** exhibited exceptional robustness in a 2 L scale-up homopolymerization at 150 °C, maintaining catalytic activity exceeding 10^7 g·mol^{-1}·h^{-1}. This demonstration of thermal stability and high productivity highlights its significant potential for application in the high-temperature solution copolymerization of ethylene with polar monomers.

While steric bulk enhances the thermal stability, incorporating stimuli-responsiveness offers dynamic control over the catalytic environment. Jiang *et al.* introduced a photoswitchable dinuclear Ni platform bridged by a stiff-stilbene (1,1′-biindane) unit; *E*↔*Z* isomerization at 365/405 nm reversibly modulated the Ni···Ni distance, steric environment, and electronic coupling (Fig. 5).[72] In ethylene/VTMS copolymerization, dinuclear (*Z*)-Ni-**9** afforded superior incorporation compared with its (*E*)-isomer (3.1 mol% versus 1.7 mol%). Notably, the (*Z*)-form uniquely enabled ethylene/MA copolymerization, whereas the (*E*)-analog was inactive. Mechanistic studies suggested that the proximal Ni centers in the *Z*-isomer facilitated cooperative coordination of the polar monomer, thereby mitigating single-site poisoning and enhancing uptake.

Expanding the utility of bimetallic cooperativity beyond photoswitching to functional tolerance, Tang *et al.* exploited the Ni···Ni cooperativity to enable the direct copolymerization of ethylene with protic monomers without prior masking.[73] Inspired by a tetranuclear precursor, the dinuclear catalyst **10b** (Ni···Ni separation=3.259 Å), activated by Et_2AlCl, effected ethylene/acrylic acid (AA) copolymerization, delivering an activity of 3.0×10^5 g·mol^{-1}·h^{-1} and 2.6 mol% incorporation at 30 °C, while retaining catalytic stability up to 90 °C (Fig. 6). DFT calculations suggested that bimetallic cooperation lowered the insertion barrier and facilitated carboxylate dissociation *via* proton transfer, thereby preventing chelation-driven deactivation. Furthermore, catalyst **10** enables an unusual tandem ethylene/acrylamide (AAm) copolymerization to furnish cyanated polyethylene (>99% —CN selectivity) with activities reaching 4.1×10^6 g·mol^{-1}·h^{-1}.[74] Mechanistic studies supported a sequence involving 2,1-insertion followed by Et_2AlCl-promoted dehydration/isomerization, which effectively converted the amide functionality to a nitrile, thereby circumventing permanent catalyst poisoning.

2.3 [P,O] Ni Catalysts

[P,O]-type Ni catalysts, including phosphine-sulfonate, phosphine-phenolate, phosphine-enolate, and bisphosphine monoxide (BPMO) families, represent a premier platform for direct ethylene/polar-monomer coordination-insertion copolymerization. In these motifs, the anionic X-type O-donor (phenolate, sulfonate, or enolate) provides a robust *σ*-anchor that stabilizes the Ni center and enhances polar tolerance, while the neutral P-donor modulates electron density and steric shielding; this soft P–hard O complementarity effectively suppresses chain transfer by creating an electronic asymmetry that stabilizes the active site against polar-group poisoning, elevating MW and enabling significant comonomer incorporation.[75]

2.3.1 Bisphosphine monoxide Ni catalysts

Systematically developed by Nozaki *et al.*, the BPMO family constitutes a hybrid P/O donor class characterized by an asymmetric P,O coordination environment. In this motif, an oxidized P=O moiety serves as the robust O-donor paired with a neutral phosphine, effectively implementing the "soft P–hard O" strategy to achieve high catalytic performance.[76–79]

Wang *et al.* addressed the intrinsically poor chain-initiation efficiency of allyl-Ni catalysts by preparing 2-methylallyl-initiated BPMO Ni complex **11** (Fig. 7).[80] The 2-methylallyl motif was found to improve initiation, presumably because increased steric bulk weakened chelation of the initiator to the

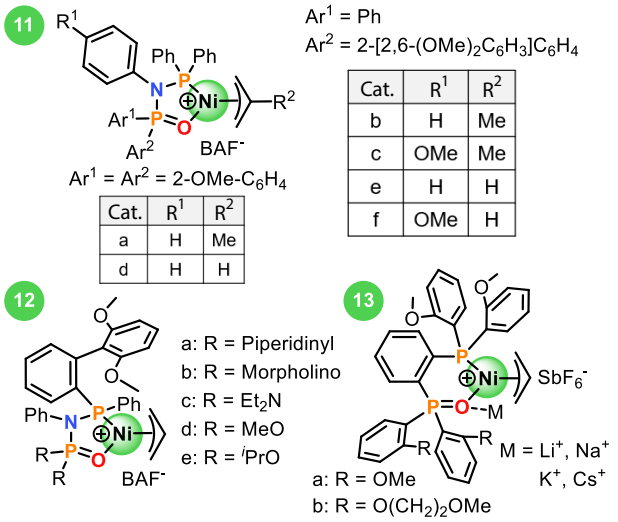

Cat.	R^1	R^2
b	H	Me
c	OMe	Me
e	H	H
f	OMe	H

Cat.	R^1	R^2
a	H	Me
d	H	H

Fig. 7 Bisphosphine monoxide Ni catalysts.

Ni center, and *ortho*-substituted diaryl variant **11b** achieved the best performance in ethylene polymerization with an activity of 4.0×10^6 g·mol^{-1}·h^{-1}. Notably, these catalysts also promote ethylene/MA copolymerization, affording MA incorporation of up to 7.0 mol% with predominantly in-chain insertion. Shifting focus from the initiating group to the electronic tuning of the ligand skeleton, Tan and co-workers investigated substituent effects on the phosphorus atom to tune the polymerization behavior of Ni catalysts **12**.[81] The incorporation of a methoxy group (**12d**) lowered the Mulliken electron density at the nickel center and accelerated ethylene insertion, delivering an activity of 1.0×10^4 g·mol^{-1}·h^{-1}, yielding EMA with an M_n of 6.6 kg·mol^{-1} and 2.2 mol% incorporation. DFT calculations correlated the experimentally observed activity increase with the reduced Mulliken charge at the Ni center induced by the substituent.

In addition to electronic modulation, restricting conformational freedom has been pursued to enhance catalyst robustness. Do and co-workers developed Ni catalysts **13** by combining ligand rigidification (*via ortho*-aryl substitution) with secondary metal cation modulation (Fig. 7).[82] By restricting the conformational dynamics in solution, the optimized catalyst **13b** achieved an ethylene/MA polymerization activity of 2.8×10^4 g·mol^{-1}·h^{-1}. Coordination of Li^+ to pendant ether oxygens on **13b** further enhanced the activity to 8.1×10^4 g·mol^{-1}·h^{-1} and enabled 4.5 mol% MA at a higher monomer concentration (1.0 mol·L^{-1}). Although it exhibited a slightly lower activity, the **13b**/Na^+ variant delivered the highest MA incorporation of 8.1 mol%. Mechanistic studies indicated that ligand rigidification improved thermal stability and suppressed chain transfer, while secondary-cation binding increased metal electrophilicity, thereby facilitating polar monomer coordination and insertion.

2.3.2 Phosphine-carbonyl Ni catalysts

Jian *et al.* introduced an "N-bridge" strategy for [P,O] Ni catalysts, replacing a weak ketone linker with a coordinating amide and generating P-carbonyl Ni catalysts **14** (Fig. 8).[83] The N-bridged **14a** enabled MA incorporation of 3.3 mol%, but exhibited low activity and low polymer MW. The introduction of bulky aryl substituents afforded catalyst **14c**, which retained MA in-

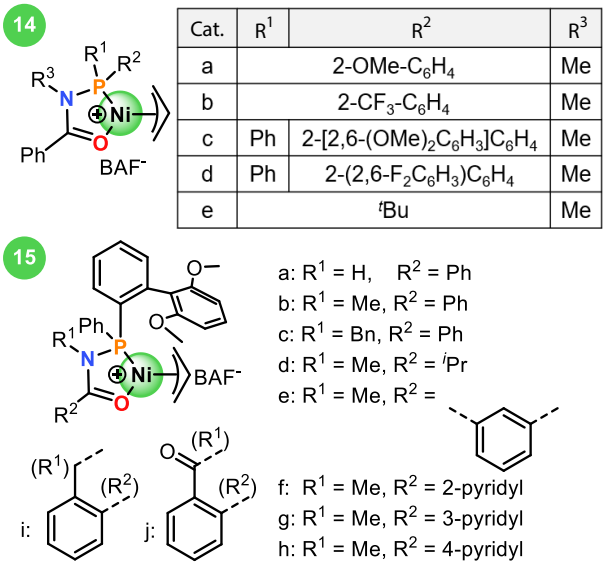

Cat.	R^1	R^2	R^3
a	2-OMe-C_6H_4		Me
b	2-CF_3-C_6H_4		Me
c	Ph	2-[2,6-$(OMe)_2C_6H_3$]C_6H_4	Me
d	Ph	2-(2,6-$F_2C_6H_3$)C_6H_4	Me
e	^{t}Bu		Me

Fig. 8 Phosphine-carbonyl Ni catalysts.

corporation (1.8 mol%) while boosting polymerization activity to 8.3×10^3 g·mol^{-1}·h^{-1} and increasing copolymer M_n to 14.1 kg·mol^{-1}. Catalyst **14c** also copolymerized ethylene with butyl vinyl ether (BVE) (incorporation: 2.0 mol%; M_n: 4.6 kg·mol^{-1}). Mechanistic studies attributed these improvements to reinforced [P,O] chelation and increased steric shielding, which suppressed oligomerization and chain transfer. Tan *et al.* extended this framework, showing that electron-donating isopropyl groups (**15d**) suppressed β-H elimination, raising polyethylene M_n to 183.6 kg·mol^{-1} (Fig. 8).[84] When applied to ethylene/MA copolymerization, a low-steric indolinone scaffold (**15i**) delivered the highest activity (4.0×10^4 g·mol^{-1}·h^{-1}) but lower M_n (37.5 kg·mol^{-1} versus 48.7 kg·mol^{-1}) and MA incorporation (1.1 mol% versus 1.6 mol%) compared to the bulkier phenyl analogue **15b**, illustrating that reduced framework sterics enhanced ethylene coordination and activity yet tended to promote chain transfer and weaken polar-monomer capture. Such trade-offs underscore the need to balance the framework rigidity and electronic effects for the target polar monomers.

To further modulate ligand hemilability, a "ring-closure" (or cyclizing) strategy was subsequently applied to construct P–carbonyl Ni catalysts **16** featuring five-, six-, and seven-membered N-rings (Fig. 9).[85] Catalytic performance increased with ring size: the seven-membered **16d** exhibited optimal behavior at 30 °C (activity: 3.3×10^3 g·mol^{-1}·h^{-1}; M_n: 1.8 kg·mol^{-1}; MA incorporation: 3.1 mol%), whereas **16c** (six-membered) was far less active, and a noncyclic reference

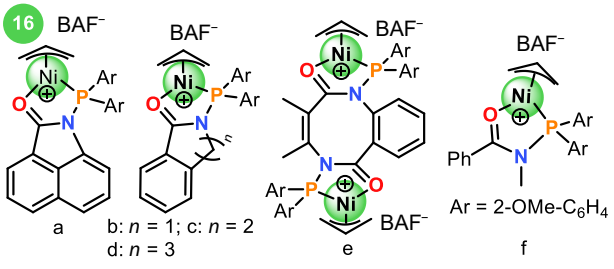

Fig. 9 Phosphine-carbonyl Ni catalysts.

(**16f**) gave similar incorporation but substantially lower MW. Structure-property analysis indicated that longer methylene bridges increased the N-donor electron density, stabilized carbonyl→Ni coordination, and, together with added steric bulk, suppressed chain transfer, thus enabling simultaneous gains in activity and MW.

2.3.3 Phosphine-phenolate Ni catalysts

Originating from neutral SHOP-type complexes, [P,O] Ni catalysts have evolved into premier platforms for ethylene/polar-monomer copolymerization.[86,87] Foundational work by Klabunde *et al.* enabled the incorporation of spacer-separated functional olefins, while Gibson *et al.* demonstrated MMA tolerance.[88,89] Following stability improvements *via* backbone aromatization,[90] Li *et al.* achieved high ethylene polymerization activity (1.1×10^7 g·mol^{-1}·h^{-1}) and produced UHMW polynorbornene using well-defined complexes.[91,92] Concurrently, Shimizu *et al.* highlighted the critical role of aryl substituents in governing acrylate insertion.[93] More recently, attractive Ni-aryl interactions have been shown to suppress *β*-H elimination.[94] Collectively, these studies underscore steric and electronic tuning as the central design principles; building on these insights, representative state-of-the-art variants are discussed below.

Since 2012, Li *et al.* systematically investigated phosphine-phenolate Ni catalysts and found that increasing the steric bulk at the phenoxide *ortho* positions exerted a negligible impact on the polymerization activity, whereas steric tuning at the phosphine substituent proved decisive for both ethylene homo- and co-polymerization performance.[50,91,92,95] Switching the aryl scaffold from phenyl to naphthyl, they prepared C8-substituted phosphine-naphtholate Ni complexes **17** (Fig. 10).[50,96] DFT calculations indicated that the naphtholate backbone was more electron-withdrawing than phenoxide (Ni partial charge: +0.289 versus +0.279), which enhanced the electrophilic activation of ethylene. For ethylene/MA copolymerization, the C8-phenyl derivative **17b** afforded MA incorporation of 3.7 mol% while exhibiting a polymerization activity of 3.7×10^5 g·mol^{-1}·h^{-1} (versus 2.8×10^4 g·mol^{-1}·h^{-1} for its phenoxide analogue). Reducing steric congestion (**17a**) further increased MA incorporation to 7.6 mol% and enabled copolymerization with dimethyl itaconate (DMI), producing linear polyethylene with difunctional end-groups. To counteract the naphthyl scaffold's tendency to promote *β*-H elimination and lower MW, Li *et al.* developed phosphine-dihydronaphtholate catalysts **18**.[97] The bulky axial-substituted **18c** performed best in ethylene/MA copolymerization, delivering high activity (2.5×10^4 g·mol^{-1}·h^{-1}) and molecular weight (M_w=35.8 kg·mol^{-1}) at 0.1 mol·L^{-1} MA, significantly outperforming less hindered **18a**, and achieving 8.2 mol% incorporation at 0.8 mol·L^{-1} MA with a relatively high M_w (11.8 kg·mol^{-1}) despite reduced activity (3.0×10^3 g·mol^{-1}·h^{-1}). Mechanistic work attributed these improvements to axial steric shielding, which favored the in-chain insertion of polar monomers over terminal insertion.

Beyond phosphorus substituents, groups positioned adjacent to the phenoxide oxygen proved equally decisive. Building on the seminal axially sterically hindered catalyst (**23-ref**) reported in 2018, an *ortho*-CF_3 modified catalyst (**19**) was applied to ethylene/allyl acrylate (AIA) copolymerization (Fig.10) to furnish copolymers containing five- and six-membered polar rings.[50,98] Under 1 MPa ethylene and 0.1 mol·L^{-1} AIA, the catalyst produced copolymers with M_w values up to 59.4 kg·mol^{-1} (versus 19.5 kg·mol^{-1} for a phosphine–sulfonate Pd benchmark), with AIA incorporation tunable between 1.0 and 5.2 mol%. Mechanistic analysis revealed distinct selectivity between acrylate and allylic double bonds (2,1- versus 1,2-insertion), enabling the coexistence of pendant allyl/acrylate units and lactone motifs. Remote electronic tuning proved similarly effective: an *ortho*-CF_3 substituted Ni catalyst (**20b**) outperformed an *m*-xylene analog (**20c**), delivering a polymerization activity of 5.0×10^4 g·mol^{-1}·h^{-1} with an MA incorporation of 1.7 mol% and an M_n of 147 kg·mol^{-1}.[99] The same catalyst also catalyzed ethylene/VTMS copolymerization to produce copolymers with M_n values up to 267 kg·mol^{-1} (activity: 5.0×10^4 g·mol^{-1}·h^{-1}; incorporation: 0.1 mol%). Together, these studies emphasized the synergistic roles of remote electronic tuning and Ni···O noncovalent axial shielding in preserving the high MW and polar-monomer tolerance.

While *ortho*-substituents critically govern steric shielding,

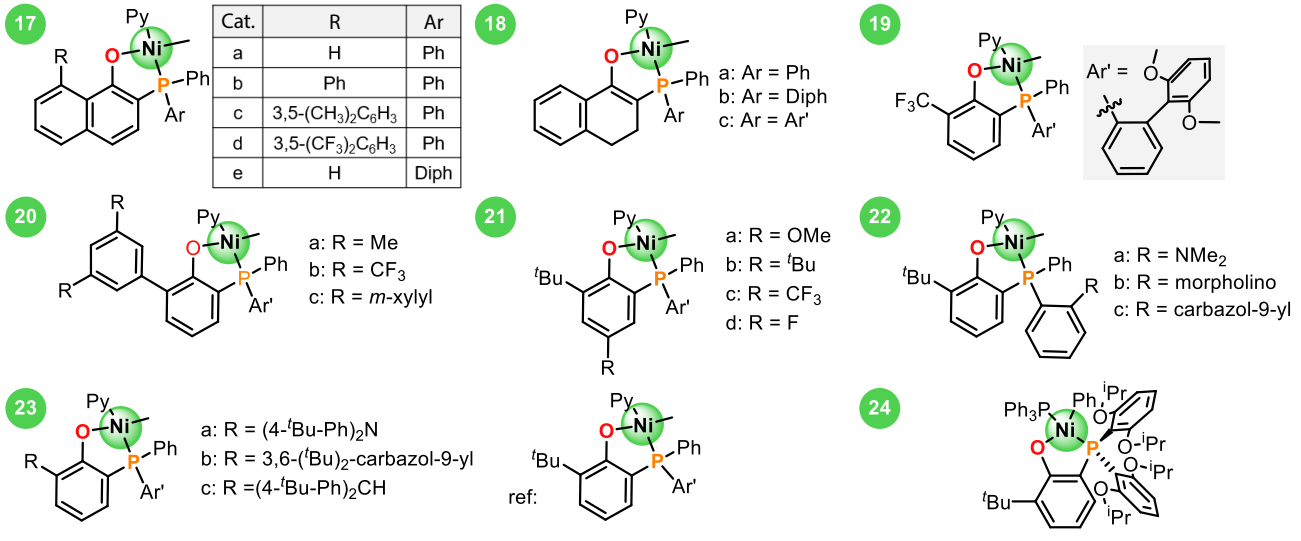

Fig. 10 Phosphine-phenolate Ni catalysts.

https://doi.org/10.1007/s10118-026-3621-x

the electronic properties of the ligand backbone can be finely tuned at remote positions. The influence of *para*-substituent effects on phosphine-phenolate Ni catalysts **21** was investigated by Zou *et al.*, who found that electron-donating groups (—OMe and —^{t}Bu) outperformed electron-withdrawing analogs (Fig. 10).[100] Catalyst **21b** (^{t}Bu) delivered the highest ethylene/MA activity (3.6×10^4 g·mol^{-1}·h^{-1}) and 1.7 mol% incorporation. When applied to the copolymerization of ethylene and *tert*-butyl acrylate (*t*BA), this complex delivered a peak activity of 6.4×10^4 g·mol^{-1}·h^{-1} with an M_n of 51 kg·mol^{-1}. Mechanistic analysis suggested that electron donors increased the electron density at the Ni center to suppress *β*-H elimination, whereas electron-withdrawing groups enhanced the oxophilicity and promoted catalyst poisoning. Subsequently, a Lewis acid modulation strategy was employed, incorporating N donors to coordinate external acids (*e.g.*, $Zn(OAc)_2$), thereby increasing steric congestion (Fig. 10).[101] For the copolymerization mediated by **22c**, $Zn(OAc)_2$ addition raised polymer M_n (from 22.3 kg·mol^{-1} to 32.8 kg·mol^{-1}) while maintaining activity (1.6×10^5 g·mol^{-1}·h^{-1}) and MA incorporation (1.2 mol%). Notably, the system tolerated temperatures up to 150 °C in ethylene/tBA copolymerization (activity: 2.4×10^5 g·mol^{-1}·h^{-1}; M_n: 9.3 kg·mol^{-1}), as the induced steric shielding suppressed thermally driven chain transfer. Finally, similar N donors were introduced at the *ortho*-position of the phenoxy group to enhance the thermal robustness of the phosphine-phenolate Ni catalysts (Fig. 10).[50,102] At 120 °C, the carbazole-substituted catalyst **23b** achieved a polymerization activity of 5.6×10^4 g·mol^{-1}·h^{-1}, with 2.8 mol% MA incorporation and an M_n of 14.2 kg·mol^{-1}, significantly outperforming the benchmark **23-ref** (activity: 1.6×10^4 g·mol^{-1}·h^{-1}; incorporation: 1.7 mol%). This 3.5-fold increase in activity confirms that combining electron donation with steric protection effectively shields the metal center against thermal and polar group deactivation.

To further push the limits of molecular weight while maintaining high activity, Jian *et al.* further increased the steric bulk of the phosphine donor to resolve the activity/MW trade-off in ethylene/acrylate copolymerization (Fig. 10). The resulting catalyst **24**, featuring bulky isopropoxy substituents, delivered exceptional activity (4.0×10^6 g·mol^{-1}·h^{-1}) and ultra-high MWs (M_n: 1000–2700 kg·mol^{-1}), overcoming traditional limitations.[103,104] Mechanistic analysis indicated that, although the bulky isopropoxy groups limited *t*BA incorporation (<1.0 mol%), these substituents effectively suppressed *β*-H elimination, thereby preserving chain growth. Consequently, the resulting UHMW copolymers displayed outstanding mechanical properties, achieving a tensile strength of 44 MPa (comparable to UHMWPE) with an elongation at break of 450%, which increased to 147 MPa after drawing (draw ratio = 3.1).

Beyond pursuing ultra-high molecular weights at mild temperatures, significant efforts have been directed toward improving the catalyst performance at industrially relevant elevated temperatures. Over the past five years, Agapie's group has concentrated on the high-temperature Ni-catalyzed copolymerization of ethylene with acrylates, making significant strides in ligand design for [P,O]-type catalysts, particularly phosphine-phenolate and phosphine-enolate systems. To address the trade-off between activity and comonomer incorporation, Agapie *et al.* introduced an "O-side steric bulk" strategy. Comparing a POP-Ni catalyst bearing hemilabile methoxy side chains (**25**) with a rigid naphthyl-backbone analog (**26**), they found that the flexible catalyst **25** exhibited superior performance at 90 °C: an activity of 6.6×10^5 g·mol^{-1}·h^{-1}, 2.11 mol% tBA incorporation, and an M_w of 55.1 kg·mol^{-1} (Fig. 11).[105] In contrast, rigid **26** maintained thermal stability but suffered from a lower incorporation (0.73 mol%), and M_w (10.1 kg·mol^{-1}). Kinetic experiments and DFT calculations attributed the enhanced incorporation to faster ether-assisted *cis-trans* isomerization that placed the growing alkyl trans to P and lowered the insertion barrier, a process facilitated by the more flexible coordination sphere of the POP variant. Building on catalyst **25**, Agapie *et al.* explored the heterobimetallic modulation.[106] They found that the $ZnCl_2/ZnBr_2$ coordination to side-chain phosphine produced a crystallographically observed "diamond core", which occupied vacant coordination sites (on Ni) and blocked olefin binding, thereby causing catalyst deactivation. In contrast, the *in situ* addition of $Al(O^iPr)_3$ raised polymerization activity by 60% (to 9.4×10^5 g·mol^{-1}·h^{-1}) while maintaining 2.2 mol% *t*BA incorporation and high MW, an effect attributed to sub-

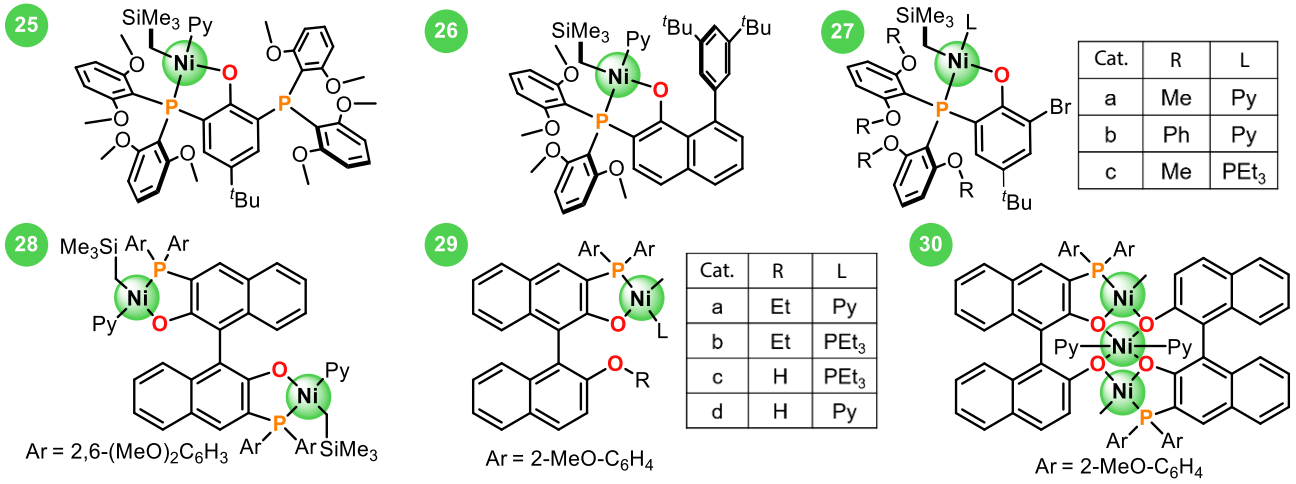

Fig. 11 Phosphine-phenolate Ni catalysts.

https://doi.org/10.1007/s10118-026-3621-x

tle steric/electronic modulation rather than strong side-chain binding.

To elucidate the termination pathways, Agapie *et al.* compared the catalysts with different axial shields (Fig. 11).[75,107] A highly shielded phenoxy derivative (**27b**) displayed exceptional activity (3.7×10^7 g·mol^{-1}·h^{-1}) at 130 °C in a 550 mL batch reactor, yielding a copolymer with low tBA incorporation (0.3 mol%) and an M_n of 15.6 kg·mol^{-1}. This performance underscores the catalyst's scalability potential, as maintaining high productivity at elevated temperatures is a prerequisite for industrial solution-phase copolymerization processes. Notably, a novel Ni-alkyl complex derived from **27b**, which was generated after acrylate-induced β-H elimination and subsequent acrylate reinsertion, was identified and characterized by crystallography. Experimental studies showed that β-H elimination rates increased with comonomer steric bulk and were modulated by labile ligand concentration, indicating that strong axial protection blocked decomposition, albeit at the cost of reduced comonomer uptake.

Inspired by enzyme-like multimetallic sites, Agapie *et al.* developed a single-component dinickel catalyst (**28**) (Fig. 11).[30,108] At 90 °C, catalyst **28** produced high-M_w copolymers (up to 85.1 kg·mol^{-1}) with tBA incorporation reaching 6.1 mol%, although the activity remained moderate (2.4×10^5 g·mol^{-1}·h^{-1}). The subsequent addition of $NaBArF_4$ to generate a **28**-Na$^+$ species substantially increased activity (to 8.2×10^5 g·mol^{-1}·h^{-1}, condition-dependent maxima higher) while lowering incorporation (0.8 mol%) and M_n (31.7 kg·mol^{-1}), a behavior rationalized by rapid substoichiometric Na$^+$ exchanges that shift the balance between chain growth and β-H elimination. To explore alternative chiral backbones for microstructure control, Guironnet *et al.* prepared BINOL-derived mono- and trinuclear Ni complexes (**29** and **30**) and showed that masking non-coordinating phenol OH groups as ethyl ethers prevented the formation of low-activity trinuclear species **(30)** (Fig. 11).[109] The resulting mononuclear complex **29b** (the ethyl-ether derivative bearing PEt_3) performed best: at 90 °C and 0.2 mol·L^{-1} MA, this complex delivered 7.9 mol% MA incorporation with an activity of 6.5×10^4 g·mol^{-1}·h^{-1}. In contrast, analogs retaining free phenols (**29c** and **29d**) suffered from intramolecular H-bonding or aggregation into inactive trinuclear forms, thereby reducing MA incorporation to about 1.0 mol%. Additionally, PEt_3 ligands offered superior process control compared to pyridine analogs, which induced uncontrolled exothermic behavior.

In addition to conventional electronic and steric modulation, Agapie *et al.* introduced a "catalyst-editing" strategy involving pendant phosphine alkylation followed by anion exchangeto access cationic catalysts **31** (Fig. 12).[110] For ethylene/tBA copolymerization at 90 °C, the methyl-substituted phosphonium **31a** achieved an activity of 1.1×10^6 g·mol^{-1}·h^{-1} and an M_w of 84.7 kg·mol^{-1}, surpassing the activity and MW using the neutral POP-Ni **25** (activity: 6.6×10^5 g·mol^{-1}·h^{-1}; M_w: 55.1 kg·mol^{-1}), albeit with lower incorporation (0.59 mol% versus 2.11 mol%). Both the phosphonium substituents and counteranions proved critical: sterically demanding cations (*e.g.*, **31g**) promoted termination and reduced MW, while the weakly coordinating tetrakis[3,5-bis(trifluoromethyl)phenyl]-borate (BAF) anion vastly outperformed trifluoromethanesulfonate (OTf) (**31h**, activity: 2.1×10^5 g·mol^{-1}·h^{-1}; M_w: 8.2 kg·mol^{-1}), thereby confirming that strong anion coordination competes with olefin insertion.

Transitioning from solution-phase polymerization to industrially preferred heterogeneous systems, Chen *et al.* developed an ion-anchoring strategy by tagging phosphine-phenolate Ni ligands with anionic —ONa groups to enable strong binding to inorganic supports (Fig. 13).[111] The resulting supported catalyst, **32b**-MgO, significantly outperformed its homogeneous precursor **32a** (activity: 9.6×10^4 g·mol^{-1}·h^{-1} versus 3.6×10^4 g·mol^{-1}·h^{-1}; MA incorporation: 2.5 mol% versus 1.1 mol%; M_n: 5.6×10^4 g·mol^{-1} versus 2.9×10^4 g·mol^{-1}). Performance depended on support (MgO > ZnO > Al_2O_3 > SiO_2); basic supports donated electron density through the ionic anchor, as evidenced by solid-state ^{1}H MAS NMR and FTIR spectroscopic analyses, thereby mitigating polar-group poisoning and enhancing thermal stability (up to 150 °C). Conversely, acidic SiO_2 suppressed the incorporation to 0.1 mol%. Crucially, catalyst **32b**-MgO demonstrated robust scalability for E-*t*BA copolymerization in a 2.5 L reactor at 120 °C, yielding 39.0 g of polymer with controlled particle morphology and effectively preventing the reactor fouling typical of homogeneous systems.

Building on this work, a co-anchoring strategy on MgO was developed to construct "polar bimodal" polyethylenes, successfully reconciling the trade-off between catalyst poisoning induced by polar groups (which typically depresses activi-

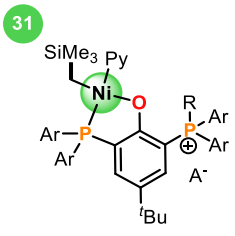

Cat.	A	R
a	BAF	Me
b	BAF	n-C_5H_{11}
c	BAF	CH_2=CH-$(CH_2)_3$
d	BAF	$(CH_2)_2$-CO_2^{t}Bu
e	BAF	4-MeC_6H_4-CH_2
f	BAF	4-CF_3-C_6H_4-CH_2
g	BAF	3,5-(^{t}Bu)$_2$$C_6H_3$-$CH_2$
h	OTf	Me

Fig. 12 Phosphine-phenolate Ni catalysts.

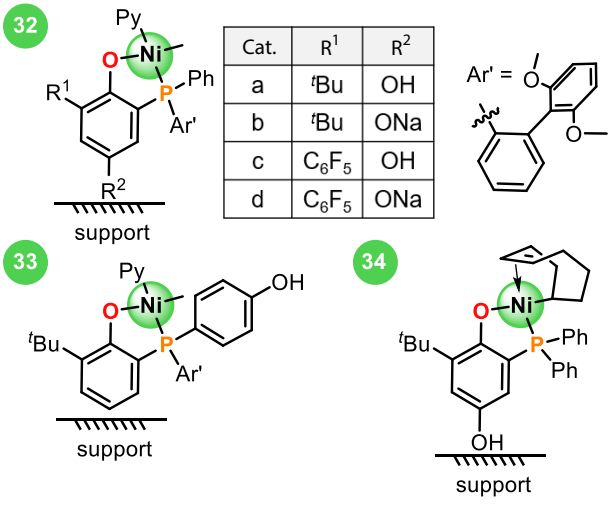

Cat.	R^1	R^2
a	^{t}Bu	OH
b	^{t}Bu	ONa
c	C_6F_5	OH
d	C_6F_5	ONa

Fig. 13 Phosphine-phenolate Ni catalysts.

https://doi.org/10.1007/s10118-026-3621-x

ty and MW) and the requirement for processable, mechanically robust polar materials.[112] This approach combines a bulky catalyst capable of producing high-MW copolymers (**33**) with a less sterically hindered catalyst that exhibits high incorporation capability (**34**) on the MgO surface. The resultant **33**/**34**–MgO system maintained a high polymerization activity (4.0×10^5 g·mol^{-1}·h^{-1}) while yielding high-molecular-weight copolymers (M_W: 5.4×10^5 g·mol^{-1}) with a *t*BA incorporation of 0.7 mol%, offering a desirable balance between processability and mechanical performance. Mechanistic studies attributed these benefits to molecular-level entanglement between the high- and low-MW fractions and the suppression of microscopic phase separation. This unique microstructure conferred high tensile strength (about 30.1 MPa) and large elongation at break (*ca.* 880%). The applicability of these bimodal resins was further validated through downstream processing scale-up, enabling the continuous extrusion of smooth filaments and the three-dimensional (3D) printing of complex polar objects, highlighting their potential for industrial additive manufacturing.

2.3.4 Phosphine-enolate Ni catalysts

To enhance the high-temperature stability of phosphine-phenolate Ni catalysts, Agapie *et al.* developed structurally analogous non-aromatic phosphine-enolate Ni catalysts **35** featuring "sandwich-type" axial shielding via *ortho*-phenoxy groups (Fig. 14).[113] At 110 °C, the optimized variant **35c** reached a copolymerization activity of 7.7×10^6 g·mol^{-1}·h^{-1}. Although *t*BA incorporation was modest (0.4 mol%–1.1 mol%), the resulting copolymers were highly linear with M_n up to 9.5 kg·mol^{-1}, significantly outperforming unshielded analogues. Mechanistic evidence linked the enhanced activity to the axial buried volume (%V_{bur}) of the ligand: large *ortho*-phenoxy groups blocked the axial coordination of carbonyl chelates, destabilized inactive resting states, and suppressed chain transfer. Conversely, strongly electron-withdrawing enolate substituents (*e.g.*, —CF_3) promoted *β*-H elimination, lowering the MW. Complementary to bidentate tuning, Agapie's team showed that modulating the labile ligand significantly improved performance: replacing strongly coordinating PEt_3 with pyridine (py) in catalyst **35c** yielded an about 5-fold activity increase (to 2.4×10^7 g·mol^{-1}·h^{-1} at 110 °C) with up to 1.6 mol% *t*BA incorporation and an M_n of 6.8 kg·mol^{-1} (Fig. 14).[107] Kinetics studies confirmed that weaker labile ligands shorten induction periods and reduced competition with olefins, thereby accelerating chain growth.

Cat.	R	Ar	L
a	Me	Ph	PEt_3
b	Me	4-CF_3-Ph	PEt_3
c	Ph	Ph	PEt_3
d	Ph	Mes	PEt_3
e	Ph	4-CF_3-Ph	PEt_3
f	Ph	3,5-(^{t}Bu)$_2$-4-OMe-Ph	PEt_3
g	Ph	Ph	Py
h	Ph	Ph	PPh_3

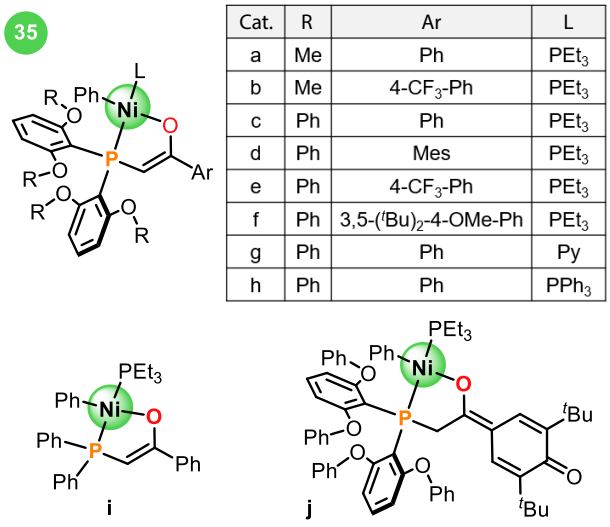

Fig. 14 Phosphine-enolate Ni catalysts.

2.4 Other Unclassified Ni Catalysts

Inspired by phosphine-phenolate Ni systems, ligand motifs were diversified to include phosphinobenzenamine and phosphine-imidate frameworks, yielding multiple new platforms.[114,115] Li *et al.* reported tunable [P,N]-type Ni catalysts **36** (Fig. 15).[114] A P-aryl, electron-withdrawing variant (**36c**) delivered notably high MA incorporation (15.5 mol% at 80 °C) while maintaining a polymerization activity of 2.3×10^4 g·mol^{-1}·h^{-1} and an M_n of 2.0×10^4 g·mol^{-1}. By contrast, an electron-donating, bulky isopropyl-substituted analogue (**36b**) showed higher activity (6.3×10^4 g·mol^{-1}·h^{-1}) but negligible MA uptake (0.12 mol%), underscoring that ligand electronics strongly govern polar-monomer affinity. Moving from bidentate frameworks to higher-denticity architectures, Gao *et al.* designed a neutral, tridentate *α*-sulfonyl *β*-diimine Ni (**37**) that combined *β*-diimine steric features with sulfonate-type electronics.[116] Complex **37a** achieved 10.2 mol% MA incorporation and an M_n of 2.28×10^4 g·mol^{-1}, overcoming the typical trade-off between high comonomer content and high MW. Mechanistic studies indicated that the sulfonate unit lowered Ni electrophilicity and provided axial protection, while DFT calculations predicted a preference for 2,1-insertion followed by chain walking, producing highly branched EMA (37–48 brs/1000C). Ancillary-ligand studies showed a clear activity trend (PhCN < MeCN < THF < ligand-free): the dimeric ligand-free species (**37e**) showed the highest activity (3.5×10^3 g·mol^{-1}·h^{-1}) and 15.6 mol% MA incorporation, whereas strongly coordinating benzonitrile (**37b**) suppressed activity (1.6×10^3 g·mol^{-1}·h^{-1}).[117]

In a distinct approach to developing neutral complexes supported by monoanionic ligands, Nett *et al.* exploited imidate tautomerization to access phosphine-imidate Ni catalysts (**38**).[115] A high-steric, electron-poor variant (**38f**) proved outstanding: at 90 °C, this complex delivered a copolymerization activity of 2.5×10^6 g·mol^{-1}·h^{-1} and an M_w of 101 kg·mol^{-1};

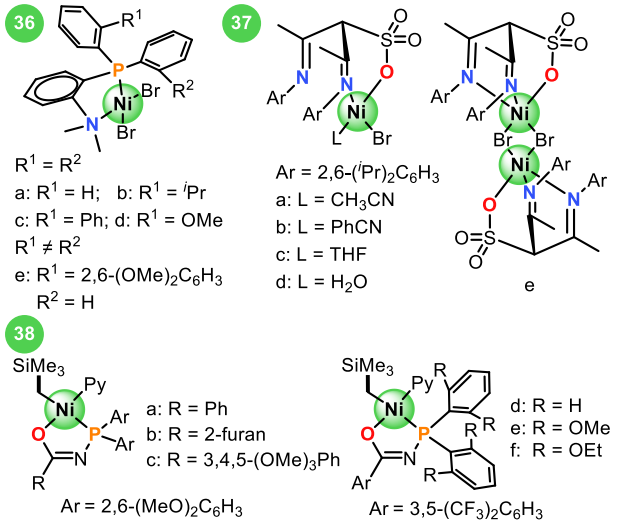

Fig. 15 Other unclassified Ni catalysts.

https://doi.org/10.1007/s10118-026-3621-x

although initial tBA incorporation was modest (0.4 mol%), optimization raised it to 2.6 mol%, demonstrating the platform's promise for high-MW, functionalized polyolefins. Mechanistic evidence suggested that hemilabile *ortho*-alkoxy coordination stabilized the Ni center, whereas the imidate form enabled high activity in a neutral framework.

3 PALLADIUM CATALYSTS

Palladium-based catalysts, notably Brookhart- and Drent-type complexes, have established the foundations of coordination-insertion copolymerization of olefins with polar monomers.[17,52] While high material and processing costs have impeded widespread industrial adoption, Pd complexes remain invaluable tools for elucidating reaction mechanisms and tailoring polymer microstructures. As d^8 late-transition-metal species, Pd(II) complexes are generally less electrophilic and less oxophilic than many d^0 early transition-metal systems (*e.g.*, Ti(IV) and Zr(IV) metallocenes).[118–120] Moreover, compared with isoelectronic d^8 Ni complexes, Pd analogs are less prone to irreversible coordination by polar functional groups and to catalyst-decomposition pathways, which helps explain Pd's typically superior comonomer tolerance and longer catalyst lifetimes in many ethylene/polar-monomer systems.[119]

3.1 [N,N] Pd Catalysts

3.1.1 α-Diimine Pd catalysts

α-Diimine Pd catalysts are prized for pronounced chain-walking; repeated alkyl migration along the growing backbone yields highly branched topologies and densely functionalized side chains, but also frequently produces largely amorphous polymers with reduced crystallinity and mechanical strength.[31,38,121–123] Thermal stability remains a critical challenge, as the free rotation of N-aryl groups can compromise axial shielding, which facilitates ligand C—H activation and *β*-H elimination, ultimately resulting in catalyst deactivation and reduction of polymer MW. To mitigate these problems, ligand design has targeted both the steric and electronic tuning of the coordination sphere. Successful strategies include the following: (i) very bulky *ortho* substituents on the N-aryl groups to restrict rotation, (ii) rigid or axially constrained backbones to maintain persistent axial protection, (iii) electronic adjustment of aryl/backbone units to balance insertion versus chain transfer, and (iv) introduction of noncovalent interactions (aryl-metal or *π*-*π* stacking) to selectively stabilize chain-growth transition states and raise the barrier to *β*-H elimination. Taken together, these approaches improved the control over branch density, polar-monomer incorporation, and product MW.[9,59,60,124]

Chen and co-workers prepared Pd catalysts **39a** featuring a combined *ortho*-diphenylmethyl substitution on the N-aryl rings together with tri-methoxy groups.[125] These modifications increased the axial buried volume from 71.6% (for the *para*-monomethoxy analog) to 79.7% and stabilized the metal center through enhanced *σ*-donation. In ethylene/MA and ethylene/AA copolymerizations, the complex produced high-MW copolymers (M_n=31.6 and 48.8 kg·mol^{-1}, respectively) but showed low comonomer incorporation (MA: 0.2 mol%; AA: 1.2 mol%), indicating that excessive axial shielding hindered polar-monomer coordination. In contrast, the trifluoro analog (**39b**) decomposed under the reaction conditions, underscoring the need to balance steric protection with insertion (Fig. 16). Pursuing an orthogonal route to increase the effective local concentration of polar monomers, Chen *et al.* added urea side chains to induce hydrogen-bonded self-assembly into dynamic multinuclear aggregates.[126] The self-assembling **40a** increased MA incorporation to 3.2 mol% (versus 0.4 mol% for the non-hydrogen-bonding control **40c**), albeit at the cost of reduced polymerization rates and lower MW.

To overcome the tendency of conventional *α*-diimine Pd catalysts to localize acrylates at the chain ends, Jian and Mecking developed a strategy utilizing a rigid dibenzo-barrelene scaffold and arylamines bearing bulky axial pentiptycenyl substituents (Fig. 16).[40] This design promoted unusual 1,2-MA insertion and facilitated chain walking by enforcing extreme axial confinement, while maintaining equatorial accessibility. Even at 90 °C, the catalyst **41** retained robust activity (1.5×10^4 g·mol^{-1}·h^{-1}), yielding high-MW EMA (M_n=85 kg·mol^{-1}; incorporation: 1.5 mol%; 158 brs/1000C). Notably, this approach ensured high main-chain functionalization (98% at 30 °C; 89% at 90 °C), affording ultra-highly branched (up to 213 brs/1000C) elastomers with polarity distributed along the backbone rather than at branch ends. Ligand design exploiting hemilabile motifs has emerged as an effective

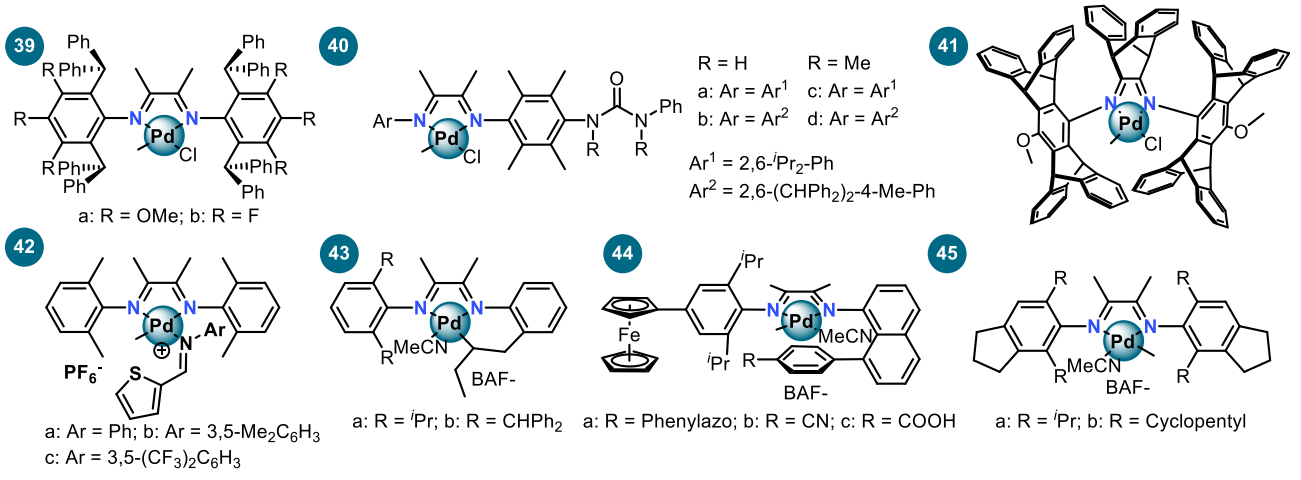

Fig. 16 *α*-Diimine Pd catalysts.

https://doi.org/10.1007/s10118-026-3621-x

approach to exert fine control over copolymer microstructures. Jian subsequently demonstrated that acrylonitrile (AN) could serve as an inert polar regulator for catalyst **41**: introducing 2000 equiv. of AN to an ethylene/MA copolymerization lowered both MA incorporation (1.5 mol% to 0.4 mol%) and activity, yet crucially reduced branching (158 brs/1000C to 49 brs/1000C) without altering the main-chain functionalization topology.[127] This modulation enabled a sequential feed route to block copolymers that combined very high- and low-branching segments. Instead of using external additives, internal ligand hemilability can be harnessed to modulate chain growth. Milani *et al.* utilized hemilabile thiophene imine Pd catalysts (**42**) to tune the insertion topology in ethylene/MA copolymerization.[128] In trifluoroethanol (TFE), the electron-deficient catalyst **42c** outperformed the electron-rich **42b** catalyst (activity: 1.0×10^4 g·mol^{-1}·h^{-1} versus 2.8×10^3 g·mol^{-1}·h^{-1}; M_n: 27.0 kg·mol^{-1} versus 14.7 kg·mol^{-1}), with both yielding 3.0 mol% incorporation. Notably, switching the solvent from acetonitrile to TFE increased the fraction of the main-chain MA units from 12% to 45%. Mechanistic studies supported by 2D NOESY NMR spectroscopy indicated that TFE formed hydrogen bonds with the inserted ester moiety, thereby stabilizing an open-chain intermediate.

In addition to modulating the chain propagation, optimizing the initiation step is critical for catalyst design. More recently, Chen *et al.* introduced allyl-pre-inserted α-diimine Pd catalysts (**43**) (Fig. 16).[129] At 30 °C, **43b** achieved an activity of 1.4×10^4 g·mol^{-1}·h^{-1}, an M_n of 14.5 kg·mol^{-1}, and 0.7 mol% MA incorporation, whereas at 80 °C, incorporation rose to 1.9 mol% while activity and M_n decreased to 6.5×10^3 g·mol^{-1}·h^{-1} and 4.9 kg·mol^{-1}, respectively. DFT calculations and mechanistic analyses indicated that *in situ* *β*-H elimination from the preinserted allyl group generated catalytically active Pd–H species. However, the substantial initial steric demand simultaneously hampered monomer insertion and promoted chain transfer, accounting for the observed activity–MW trade-off.

The introduction of stimuli-responsive functionalities into the ligand skeleton offers a dynamic avenue for catalyst control. Peng and Zou combined a redox-active ferrocene unit with stimuli-responsive substituents, including a photoswitchable azobenzene (**44a**), cyano substituent (**44b**), or carboxylic acid (**44c**) (Fig. 16).[130] Photoisomerization of **44a** (*trans*→*cis*) increased the axial steric shielding and M_n from 13.2 kg·mol^{-1} to 16.9 kg·mol^{-1}, but reduced polymerization activity from 9.3×10^3 g·mol^{-1}·h^{-1} to 6.3×10^3 g·mol^{-1}·h^{-1} and lowered MA incorporation from 2.1 mol% to 1.1 mol%. Oxidation of the ferrocene unit to ferrocenium uniformly degraded catalytic performance. Binding $B(C_6F_5)_3$ to **44b** produced a Lewis-acid–modulated steric increase that increased M_n to 16.4 kg·mol^{-1} with modest losses in activity and incorporation. Notably, coordination of Na^+ to **44c** rigidified the ligand framework *via* cation-*π* interactions and delivered concurrent gains in activity (9.0×10^3 g·mol^{-1}·h^{-1} versus 5.3×10^3 g·mol^{-1}·h^{-1}), M_n (19.7 kg·mol^{-1} versus 13.3 kg·mol^{-1}), and MA incorporation (1.5 mol% versus 1.2 mol%).

Returning to the optimization of static ligand geometry, Jian and co-workers developed a "flexibility + steric bulk" design strategy based on a 5-aminoindane core bearing axial/*ortho* cycloalkyl substituents (Fig. 16).[131] The cyclopentyl-substituted **45b** retained activity of 3.0×10^4 g·mol^{-1}·h^{-1} at 90 °C, achieved MA incorporation of 2.9 mol%, and afforded an M_w of 53 kg·mol^{-1} (MA distribution: 15% in main chain, 85% at branch ends). In comparison, the less sterically demanding isopropyl analog (**45a**) produced high-M_n copolymers at lower temperatures (50–70 °C). Mechanistic analysis attributed the thermal robustness and suppression of chain transfer to the *meta*-type axial shielding effect amplified by the cycloalkyl conformational dynamics.

Parallel to N-aryl modifications, backbone engineering has emerged as a fruitful strategy. In 2020, Gao introduced a rigid dinaphthobarrelene-based Pd catalyst (**46**) featuring a 3D confined coordination pocket (Fig. 17). At 25 °C, **46** outperformed the less hindered dibenzobarrelene-based analog,[132,133] achieving an activity of 3.8×10^4 g·mol^{-1}·h^{-1}, an M_n of 39.9 kg·mol^{-1}, and an MA incorporation of 2.0 mol%. Notably, at 50 °C, catalyst **46** achieved 5.2 mol% MA incorporation with narrow dispersity (PDI: 1.26), demonstrating that 3D confinement effectively suppresses chain transfer. The optimization of ring electronics highlighted that the electron-rich OMe-substituted catalyst (**47a**), stabilized by intramolecular C—H···OMe interactions (confirmed by single-crystal X-ray diffraction), delivered a high M_n (72.3 kg·mol^{-1}) at 25 °C and sustained activity at 80 °C with MA incorporation reaching 7.6 mol% (up to 9.5 mol% at 4.4 mol·L^{-1} MA), there verifying the cooperative benefits of electron-rich centers and ligand rigidity.[134] Alternatively, modifying backbone planarity can drastically alter the steric environment. Liu *et al.* designed de-aromatized acenaphthene ligands bearing *ortho*-di-*tert*-butyl groups to create nonplanar, high-steric-demand environments (%V_{bur} up to 63.1%) (Fig. 17).[135] While the de-aromatized framework improved the *ortho*-^{i}Pr substituted **48b** (activity: 1.4×10^3 g·mol^{-1}·h^{-1}; MA incorporation: 2.7 mol%) over its planar analogue (**48a**), application of this motif to the already congested diarylmethyl system (**48d**) proved counterproductive. Although MA incorporation with **48d** reached 2.1 mol%, excessive steric hindrance severely impeded chain propagation, reducing both the activity and MW.

To address the inherent trade-off between comonomer incorporation and MW in *α*-diimine Pd catalysts, Dai's group established a coherent design paradigm centered on two complementary strategies: "dynamic steric promotion of insertion" and "remote/axial interactions for MW enhancement"

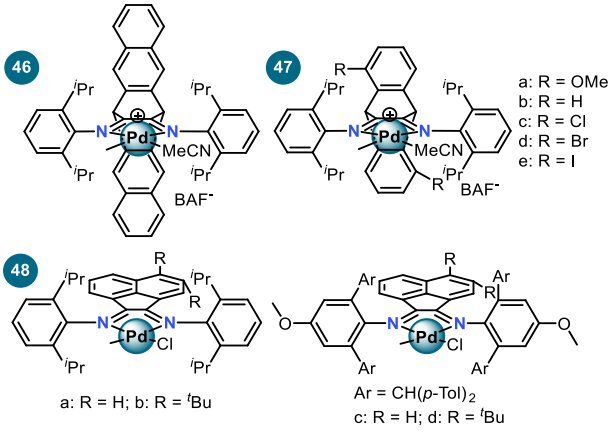

Fig. 17 *α*-Diimine Pd catalysts.

https://doi.org/10.1007/s10118-026-3621-x

(Fig. 18). Dai initially exploited flexible substituents to create dynamically adaptive active sites that balance the incorporation and MW. For instance, to address thermal deactivation in rigid systems, flexible cycloalkyl variants were found to effectively suppress ligand C—H activation: cyclohexyl-substituted **49d** achieved an activity of 1.1×10^4 g·mol^{-1}·h^{-1} and produced a high-MW copolymer (M_n: 104.6 kg·mol^{-1}; MA incorporation: 1.0 mol%).[136] Building on this, the collaborative modulation of axial sterics and backbone rigidity proved to be broadly effective. A "flexible-sandwich" design demonstrated that cyclohexyl substitution (**50b**) raised M_n relative to cyclopentyl (**50a**) (40 kg·mol^{-1} versus 24 kg·mol^{-1}).[137] Furthermore, combining a rigid dibenzobarrelene backbone with flexible axial cycloalkyls generated complementary structure-property relationships: the cyclopentyl derivative (**51a**) attained the highest MA incorporation (2.8 mol%) and branching (117 brs/1000C), while the bulkier cyclohexyl variant (**51b**) yielded the highest M_n (193.6 kg·mol^{-1}) with lower incorporation (0.85 mol%).[138] A follow-up study reinforced this trend, showing that increasing axial bulk (**52a** versus **52b**) raised activity (1.67×10^3 g·mol^{-1}·h^{-1} versus 3.3×10^3 g·mol^{-1}·h^{-1}) and M_n (20 kg·mol^{-1} versus 40 kg·mol^{-1}) but lowered MA incorporation (from 3.9 mol% to 1.5 mol%), highlighting a predictable trade-off between axial shielding and comonomer accessibility.[139]

Other geometric constraints and dynamic substituents beyond the cycloalkyls were explored. Introducing benzo-fused cyclopentyl units created open axial pockets by displacing *ortho*-aryls away from the axial trajectory, thereby promoting both chain transfer and bulky monomer insertion. As a result, **53a** achieved 20.7 mol% MA incorporation (at 4.0 mol·L^{-1} MA) but produced low-M_n oligomers (5 kg·mol^{-1}).[140] Similarly, a dynamic benzyl-substituted catalyst (**54b**, $\%V_{bur}$: 59.4%) balanced activity (6.3×10^3 g·mol^{-1}·h^{-1}) and M_n (24.4 kg·mol^{-1}) with moderate MA incorporation (1.5 mol%), confirming that modest, mobile steric bulk facilitates the coordination of bulky polar comonomers without severely penalizing chain growth.[141] Remote electronic tuning and substituent effects introduce further tradeoffs. *Para*-OMe modification of the diarylmethyl backbone (**55c**) induced ligand twisting *via* steric repulsion, increasing MA incorporation to 3.0 mol% at the expense of M_n (1.4–3.2 kg·mol^{-1}).[142]

Asymmetric substituents have also been shown to generate more open coordination spaces. The asymmetric acenaphthene catalyst **56a** (bearing an OMe group) provided an open catalytic pocket, delivering high MA incorporation (10.7 mol% at 30 °C) and hyperbranched topologies (121 brs/1000C), albeit with low M_n (3.1 kg·mol^{-1}).[143] Additionally, backbone heteroatoms modulated performance via soft/hard interactions: S-containing **57c** promoted chain transfer (low M_n: 1.6 kg·mol^{-1}) *via* soft-soft interactions, whereas O-analog **57b** enabled higher MA incorporation (2.1 mol%).[144] Furthermore, introducing a second coordination layer *via* a bridged imine-dibenzyl motif yielded **58b**, which leveraged N-atom interactions with the growing chain's β-H to suppress chain transfer/chain-walking, producing a higher M_n (13.6 kg·mol^{-1}) and incorporation (2.6 mol%) with reduced branching (48 brs/1000C) compared to the N-diphenyl control (**58a**).[145] Systematic halogenation studies revealed a delicate balance between substituent size and electronic effects:

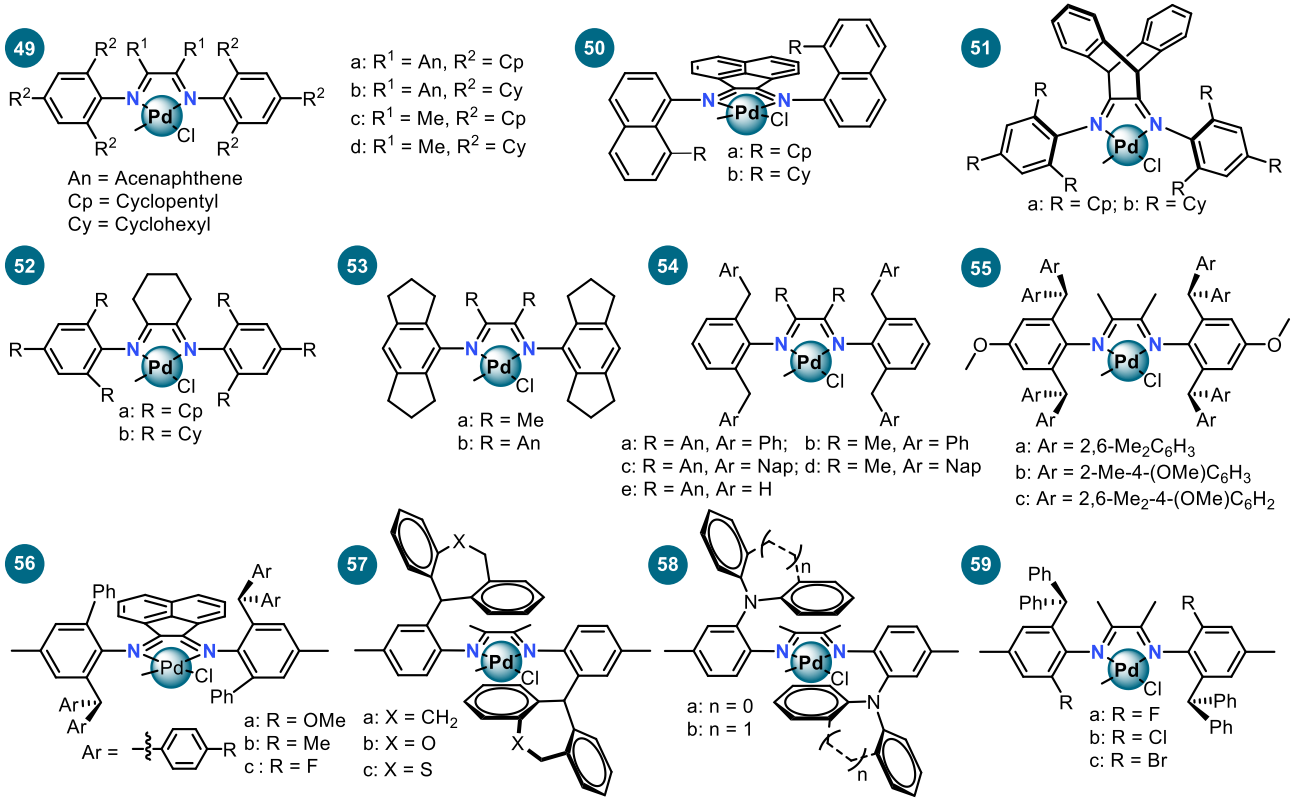

Fig. 18 *α*-Diimine Pd catalysts.

https://doi.org/10.1007/s10118-026-3621-x

the Br-substituted analogue (**59c**) significantly increased M_n (34.1 kg·mol^{-1}) but suppressed incorporation (0.7 mol%), the Cl-analogue (**59b**) yielded the highest activity in the series (1.8×10^4 g·mol^{-1}·h^{-1}), illustrating the intrinsic competition between steric shielding and comonomer access.[146]

Collectively, these studies underscore that catalyst performance is governed by a multidimensional interplay between sterics, electronics, and backbone flexibility. In general, bulky and strongly donating ligands promote activity and MW, whereas electron-deficient or spatially accessible centers favor incorporation at the cost of activity. Importantly, these goals are not mutually exclusive; precise tuning of remote sterics and axial shielding can balance high activity with substantial functionalization, offering clear design guidelines for future catalyst optimization.

3.1.2 Pyridine-imine Pd catalysts

Owing to their strong σ-donation and modularity, pyridine-imine Pd complexes are widely employed in ethylene/polar-olefin copolymerization.[9] These catalysts typically yield highly branched functionalized oligomers with high polarity. Since 2020, Dai's group has systematically explored this platform, strategically varying the substituent volume, remote electronics, and backbone flexibility to delineate the key structural parameters governing ethylene/MA copolymerization (Fig. 19).

Dai and co-workers first established how ligand substituent orientation and electronic effects dictate the copolymerization performance. Early work probed distinct axial steric motifs: compared with **60** and **61** (%V_{bur}: 50.7%), catalyst **62** (%V_{bur}: 57.4%), featuring outward-facing phenyl rings, provided enhanced axial shielding.[147] Under 4 atm ethylene and 1.0 mol·L^{-1} MA, catalyst **62** delivered an incorporation of 8.4 mol% and an M_n of 12.9 kg·mol^{-1}, substantially outperforming the inward-facing analogues. Building on this, the more sterically biased **63a** increased MA incorporation to 13.8 mol% under the same conditions, albeit with lower polymerization activity (2.6×10^3 g·mol^{-1}·h^{-1}) and reduced M_n (5.3 kg·mol^{-1}).[148] Replacing the rigid 8-phenylnaphthyl substituent with flexible alkyls (Me, *n*-Bu) likewise affected the balance of activity, incorporation, and M_n.[149] The *n*-butyl-substituted **64c** achieved 10.2 mol% MA incorporation (at 1.0 mol·L^{-1} MA), with an activity of 3.4×10^3 g·mol^{-1}·h^{-1} and M_n of 5.5 kg·mol^{-1}, surpassing the rigid 8-phenyl analogue **63b** (incorporation: 7.5 mol%). Structure-activity analysis indicated that flexible alkyl chains provided sufficient axial shielding to

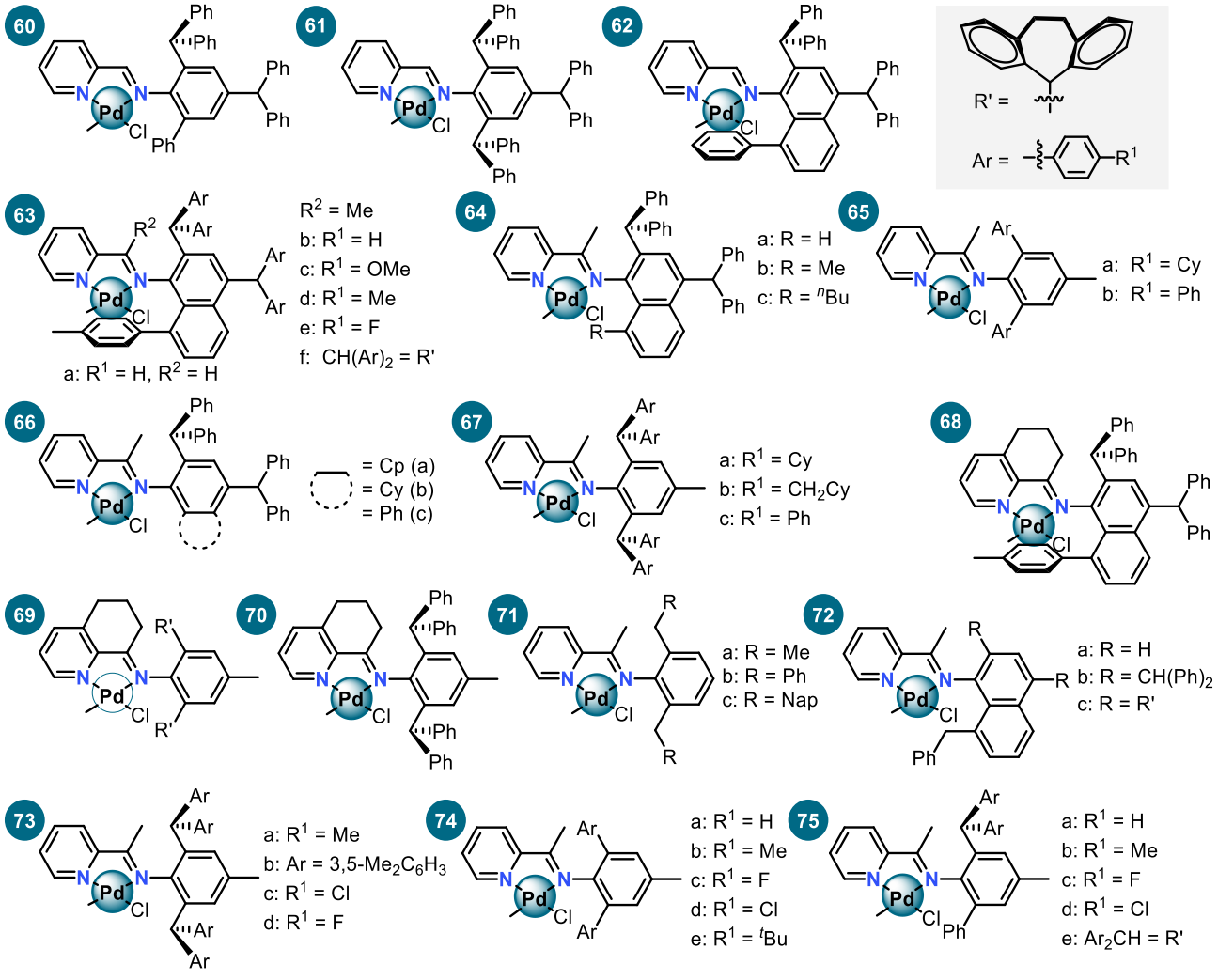

Fig. 19 Pyridine-imine Pd catalysts.

suppress chain transfer, whereas their dynamic, smaller steric footprint lowered the barrier to coordination for both ethylene and MA, enabling simultaneous gains in activity and incorporation. Similarly, catalyst **65a**, bearing a remote flexible cyclohexyl substituent, outperformed its fully rigid counterpart, **65b**.[150] At 30 °C with 1.0 mol·L^{-1} MA, the flexible **65a** gave an activity of 5.2×10^3 g·mol^{-1}·h^{-1} and 11.9 mol% MA (versus 8.5 mol% for **65b**). Notably, increasing the MA concentration to 2.0 mol·L^{-1} further raised incorporation to 19.7 mol%.

Alternative geometric constraints have also been explored. Constraining the *N*-aryl moiety with cyclic substituents forces the neighboring aryl rings away from the metal axis, thereby creating a more open axial pocket.[151] Consequently, catalyst **66a** exhibited exceptional affinity for MA, producing oligomers (M_n≈300 g·mol^{-1}) with incorporations up to 23.7 mol% and a branching density of *ca*. 159 brs/1000C. Combining remote flexible cycloalkyl groups with bulky diarylmethyl substituents also improved performance.[152] Specifically, catalyst **67b** bearing a remote cyclohexylmethyl unit combined high MA incorporation (7.1 mol%–9.6 mol%) with the highest activity (1.3×10^3 g·mol^{-1}·h^{-1}) in the series, significantly outperforming the less flexible **67c** (2.1×10^2 g·mol^{-1}·h^{-1}).

Imparting flexibility to the ligand backbone demonstrated comparable efficacy. More recent efforts have targeted the MW bottleneck *via* "rigid-flexible" hybrid and extreme-environment designs by combining a flexible backbone with distinct arylamines (**68**–**70**).[153] Catalyst **69** employed a "rotation-restricted" strategy by fusing a flexible 5,6,7,8-tetrahydro-8-quinoline backbone with bulky dibenzosuberyl substituents, which suppressed chain transfer and achieved an M_n of 49.5 kg·mol^{-1} with 4.6 mol% MA incorporation.

Further investigations into flexible monoarylmethyl substituents revealed differentiated control of insertion versus chain transfer: a sterically compact **71a** achieved the highest MA incorporation (18.3 mol%), whereas a bulky naphthylmethyl derivative **71c** limited polar coordination but markedly increased activity (6.0×10^3 g·mol^{-1}·h^{-1}) and M_n, producing hyperbranched copolymers with polar groups at long branch ends.[154] A subsequent advance employed dual-axial shielding (flexible 8-benzyl plus 2-diarylmethyl) to reconcile high incorporation and high MW. The sterically open, single-sided catalyst **72a** showed higher activity (1.1×10^4 g·mol^{-1}·h^{-1}) and incorporation (17.8 mol%), whereas the doubly shielded **72b** suppressed chain transfer and raised M_n by roughly sevenfold to 8.4 kg·mol^{-1} while maintaining adjustable incorporation (7.3 mol%–12.6 mol%).[155]

Fine-tuning of ligand electronics is equally vital. The methyl-substituted, electron-donating catalyst **73a** exhibited the highest MA incorporation (15.1 mol%) despite modest activity (9.8×10^2 g·mol^{-1}·h^{-1}) and low M_n (633 g·mol^{-1}), whereas electron-withdrawing F/Cl substituents (**73c** and **73d**) increased branching (up to 174 brs/1000C) and reduced M_n.[156] A similar electronic modulation was observed for the N-terphenyl iminopyridyl Pd catalysts.[157] Although electron-withdrawing groups (*e.g.*, Cl in **74d**) boosted the activity, the electron-donating ^{t}Bu-substituted **74e** maximized MA incorporation (19.8 mol%). These palladium species facilitated deep chain walking; notably, the electron-withdrawing F-substituted **74c** produced hyperbranched co-oligomers featuring unique "branch-on-branch" architectures and predominant long-chain branching (up to 83% of the total branches). Consistent with this trend, single-sided asymmetric catalysts generally yield low MW copolymers.[158] However, installing a bulky dibenzosuberyl motif (**75e**) imparted substantial axial steric hindrance to retain high MA incorporation (15.2 mol%) while raising M_n to 3.4 kg·mol^{-1} (homopolymer M_n up to 185.6 kg·mol^{-1}), thereby mitigating the chain-transfer liability of conventional single-sided steric designs.

Overall, increasing the steric hindrance on the aniline fragment (diarylmethyl, naphthyl, fused rings) in pyridine-imine Pd systems typically suppresses chain transfer and enhances both MW and activity, yet tends to reduce MA incorporation. Conversely, flexible or semi-sandwich substituents favor higher incorporation at the cost of a lower MW. Notably, remote electronic modulation of the pyridine-imine backbone has a limited direct impact on incorporation, but can modulate active-site stability and thus polymerization activity under specific conditions.

3.1.3 Amine-imine Pd catalysts

Amine-imine Ni and Pd catalysts utilize tunable *N*,*N*-bidentate ligands to modulate the competition between chain growth and transfer.[159–164] Specifically, in ethylene/polar-monomer copolymerizations mediated by Pd analogs, while typically yielding highly branched or low-MW products, strategies involving axial shielding and asymmetric "mixed-sandwich" designs have partially reconciled MW with incorporation, although polar-monomer tolerance and thermal robustness remain areas for improvement.

Gao *et al.* investigated electronic effects of para-substituents in catalysts **76** (Fig. 20).[165] The electron-rich catalyst **76a** achieved the best overall performance (activity: 1.4×10^3 g·mol^{-1}·h^{-1}; M_n: 12.1 kg·mol^{-1}; MA incorporation: 3.2 mol%), whereas the electron-deficient analog **76d** exhibited significantly lower activity (3.3×10^2 g·mol^{-1}·h^{-1}), M_n (4.8 kg·mol^{-1}), and incorporation (0.8 mol%). Mechanistic analysis indicated that increased electron donation reduced metal oxophilicity, thereby enhancing polar-monomer tolerance and favoring direct insertion over chain walking.

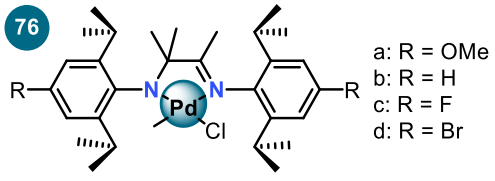

Fig. 20 Amine-imine Pd catalysts.

3.2 [N,O] Pd Catalysts

3.2.1 Anilinonaphthoquinone Pd catalysts

Cai and Shiono developed anilinonaphthoquinone–Pd systems.[166] Subsequent immobilization of these complexes on silica *via* hydrogen bonding yielded the heterogeneous catalyst **77**/SiO_2, which delivered moderate activity (2.5×10^4 g·mol^{-1}·h^{-1}) and unexpectedly high M_n (up to 98 kg·mol^{-1}) by utilizing support–ligand interactions to retard chain transfer (Fig. 21).[167] In contrast, supporting the catalyst on Lewis-acidic ^{i}Bu$_3$Al/SiO_2 (**78**) maintained comparable activity but drastically reduced both M_n

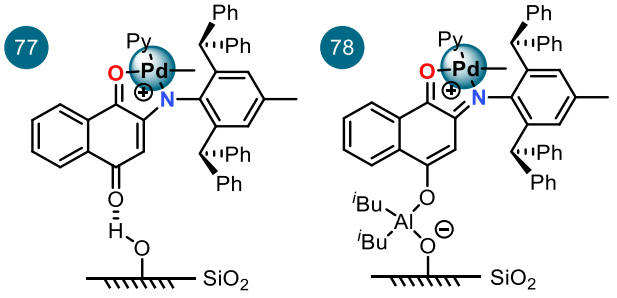

Fig. 21 Anilinonaphthoquinone Pd catalysts.

(*ca.* 5 kg·mol^{-1}) and incorporation (0.2 mol%–0.4 mol%), as the aluminum species lowered the effective electron density at the Pd center to increase olefin electrophilicity and accelerate chain transfer.[168] From a scale-up perspective, these heterogeneous strategies offer a critical advantage of strictly controlling the polymer morphology. The resulting copolymers replicate the spherical shape of the silica support, thereby effectively eliminating the stickiness and reactor fouling issues typically associated with polar copolymers produced by homogeneous analogs, making them suitable candidates for continuous industrial slurry processes.

3.3 [P,O] Pd Catalysts

3.3.1 Phosphine-sulfonate Pd catalysts

Drent-type phosphine-sulfonate Pd catalysts remain the benchmark for linear copolymer syntheses.[41,169] Modulating the steric environment serves as a key handle for tailoring catalyst properties: enhanced steric or axial bulk suppresses chain transfer to boost MW and activity, albeit often at the cost of comonomer uptake, whereas more open or flexible sterics facilitate incorporation, but typically compromise MW. Electronic effects primarily influence activity through active-site stabilization, with electron-withdrawing groups often enhancing both activity and MW, whereas direct effects on insertion selectivity are generally modest.[170,171]

Beyond the standard steric and electronic parameters, secondary interactions between the metal center and ligand pendants can provide additional stabilization. Incorporating sp^2-hybridized N-donors (carbazole and pyrrole) into phosphine–sulfonate ligands allows tuning of secondary metal–ligand interactions *via* weak Pd···N contacts (Fig. 22).[172] Single-crystal analysis of carbazole derivative **79a** revealed a contact distance of 3.56 Å that substantially improved its thermal stability. In ethylene/MA copolymerization, **79a** achieved an activity of 4.1×10^4 g·mol^{-1}·h^{-1}, M_n of 45.6 kg·mol^{-1}, and 9.3 mol% incorporation; notably, comparably high activity (3.9×10^4 g·mol^{-1}·h^{-1}) and incorporation (6.3 mol%) were sustained in ethylene/AA copolymerization. By comparison, the pyrrole analog **79b** was less active (2.0×10^4 g·mol^{-1}·h^{-1}) but achieved higher MA incorporation (13.0 mol%). The addition of $B(C_6F_5)_3$ accelerated chain transfer (up to *ca.* 670-fold), roughly doubling the activity but lowering the MW.

Complementing these secondary interaction studies, the direct modulation of steric hindrance at the phosphine donor remains a primary tool for tuning catalyst performance. By probing *ortho*-steric effects in asymmetric phosphine–sulfonate Pd systems (**80**), Jian *et al.* varied the phosphine-aryl

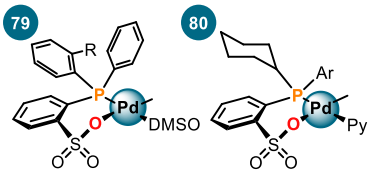

Cat.	Ar
a	2-(OMe)C_6H_3
b	2,6-$(OMe)_2C_6H_3$
c	2,4,6-$(OMe)_3C_6H_2$
d	2,6-$(O^iPr)_2C_6H_3$

a: R = Carbazole-9-yl
b: R = 2,5-Me_2-Pyrrole-1-yl

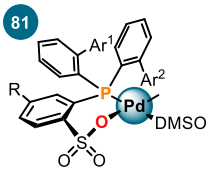

Cat.	R	Ar^1	Ar^2
a	Me	2,6-$(OMe)_2C_6H_3$	H
b	Ph	2,6-$(OMe)_2C_6H_3$	H
c	Me	2,6-$(OMe)_2C_6H_3$	
d	H	2,6-$(OMe)_2C_6H_3$	H

Fig. 22 Phosphine-sulfonate Pd catalysts.

alkoxy bulk (*o*-OMe, *o*,*o*-(O^{i}Pr)$_2$) (Fig. 22).[173] Increasing *ortho*-bulk from **80a** to **80d** produced only modest activity changes (2.2×10^4–3.1×10^4 g·mol^{-1}·h^{-1}) but raised copolymer M_n (38–63 kg·mol^{-1}) and reduced MA incorporation (4.5 mol%–3.0 mol%), a trade-off attributed to the simultaneous suppression of β-H elimination and polar-monomer coordination. An intermediate-steric catalyst (**80c**) uniquely achieved high incorporation of both MA (9.5 mol%) and AA (8.3 mol%) under low ethylene pressure, outperforming more hindered analogues.

Remote ligand tuning *via para*-substitution on the sulfonate aryl (**81a**–**81c**) was applied to enhance polymerization performance (Fig. 22).[174] By adjusting the active-site charge and buried volume, the highly conjugated **81b** excelled in copolymerizing ethylene with ethylene glycol methyl ether acrylate (EGMA), achieving high activity (3.6×10^6 g·mol^{-1}·h^{-1}) and molecular weight (M_n=221 kg·mol^{-1}), along with the incorporation of 0.87 mol%. Consequently, the resulting copolymer exhibited exceptional tensile properties (elongation at break: 974%; strength: 45 MPa) and could be further crosslinked *via* a third monomer (5-vinyl-2-norbornene) to enhance the elastic recovery.

To access vitrimer-capable polyolefins, catalyst **81d**, bearing bulky axial substituents, was utilized to copolymerize ethylene with acetoacetoxyethyl acrylate (AAEA), yielding an activity of 2.20×10^5 g·mol^{-1}·h^{-1}, an M_n of 235 kg·mol^{-1}, and 0.6 mol% incorporation (Fig. 22). A structurally similar norbornene-derived comonomer delivered significantly higher incorporation (9.5 mol%); this high incorporation, combined with the acetoacetate side chains, facilitated dynamic covalent crosslinking, producing vitrimer networks with balanced thermo-mechanical and reprocessing performance.[45,175]

3.3.2 Bisphosphine monoxide Pd catalysts

BPMO ligands have emerged as a versatile class of [P,O] chelates for Pd-catalyzed ethylene/MA copolymerization. Nozaki's seminal work established that cationic BPMO–Pd complexes could copolymerize ethylene with various vinyl polar monomers to yield linear copolymers, albeit with lower activities than those of phosphine-sulfonate systems.[76,77] However, the inherent modularity of the BPMO scaffold, which offers multiple sites for steric and electronic modification, has motivated extensive structural optimization aimed at bridging this performance gap.[78,176]

By exploiting asymmetric benzothiophene-based frameworks, Jian *et al.* demonstrated the critical importance of balancing the P-substituent sterics and electronics (Fig. 23).[177] While the sterically exposed variant **82a** (%V_{bur}: 45.6%) proved inactive in ethylene/MA copolymerization, the electron-donating *o*-methoxy-phenyl derivative **82b** (%V_{bur}: 48.2%) achieved an optimal balance, delivering an activity of 1.6×10^4 g·mol^{-1}·h^{-1} with 3.4 mol% incorporation, alongside effective copolymerization of AA (2.6 mol% incorporation) and AN (0.8 mol% incorporation). In contrast, the electron-deficient fluoro-derivative **82c** and excessively bulky **82d** exhibited diminished performance. Subsequent investigations into the electronic nature of the P=O donor revealed distinct structure–property relationships.[176,178] The electron-deficient catalyst **83a** produced a low-M_n copolymer (1.3 kg·mol^{-1}), which was attributed to a weak *trans* effect that amplified chain transfer. Conversely, employing a strongly donating phosphoramidate (**83e**) increased the electron density at the Pd center, effectively suppressing *β*-H elimination. This electronic modulation (**83e**) substantially improved MA copolymerization performance—yielding an activity of 1.5×10^4 g·mol^{-1}·h^{-1}, 5.0 mol% incorporation, and an M_n of 7.4 kg·mol^{-1}—and expanded the substrate scope to include BVE (0.4 mol%), VAc (0.3 mol%), and AN (1.0 mol%), confirming that enhancing P=O donation within a bulky scaffold is a viable strategy for raising MW and broadening tolerance.

To expand the structural diversity further, an indole-bridged N(sp^2)—C(sp^2) BPMO catalyst (**84**) was introduced.[179] A clear trade-off was observed: while the sterically encumbered catalyst **84b** excelled in ethylene homopolymerization (activity: 5.6×10^6 g·mol^{-1}·h^{-1}; M_n: 81.6 kg·mol^{-1}), this complex failed to copolymerize ethylene with MA. In contrast, the strongly donating dimethylamino-substituted analog **84f** displayed superior functional group tolerance, catalyzing ethylene/MA copolymerization with activity of 1.8×10^4 g·mol^{-1}·h^{-1} and 3.3 mol% incorporation. Moreover, **84f** successfully incorporated BVE (incorporation: 0.3 mol%; M_n: 5.1 kg·mol^{-1}) and AN, demonstrating that pairing an indole scaffold with strong P=O donation significantly enhanced copolymerization capability.

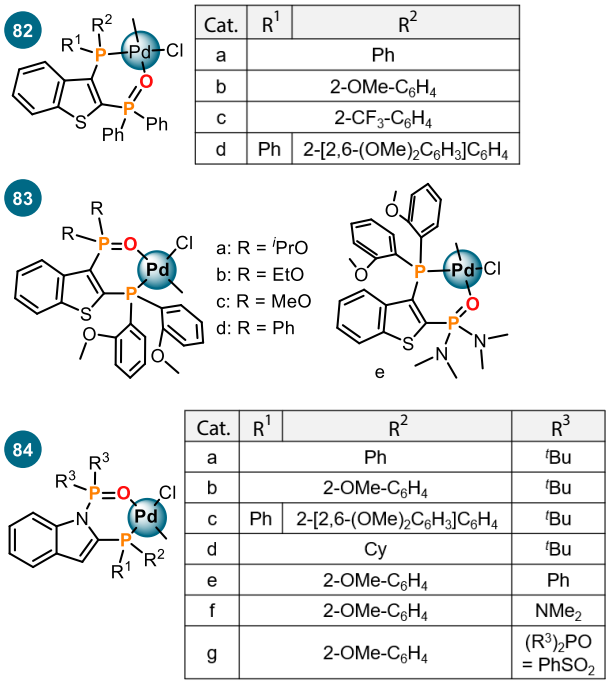

Cat.	R^1	R^2
a		Ph
b		2-OMe-C_6H_4
c		2-CF_3-C_6H_4
d	Ph	2-[2,6-$(OMe)_2C_6H_3$]C_6H_4

Cat.	R^1	R^2	R^3
a		Ph	^{t}Bu
b		2-OMe-C_6H_4	^{t}Bu
c	Ph	2-[2,6-$(OMe)_2C_6H_3$]C_6H_4	^{t}Bu
d		Cy	^{t}Bu
e		2-OMe-C_6H_4	Ph
f		2-OMe-C_6H_4	NMe_2
g		2-OMe-C_6H_4	$(R^3)_2PO$ = $PhSO_2$

Fig. 23 Bisphosphine monoxide Pd catalysts.

3.3.3 Phosphine-carbonyl Pd catalysts

Extending the N-bridge concept from Ni to Pd analogs, Jian *et al.* employed these rigid phosphine-amide ligands to enforce intramolecular [P,O] chelation (Fig. 24).[83] The sterically bulky biphenyl-substituted catalyst **85c** achieved the best balance in ethylene/MA copolymerization (activity: 6.7×10^3 g·mol^{-1}·h^{-1}; M_w: 6.1 kg·mol^{-1}; incorporation: 2.4 mol%). In contrast, the less hindered **85b** yielded lower activity and MW but exhibited a broader substrate scope. This catalyst successfully copolymerized BVE with an activity of 5.0×10^4 g·mol^{-1}·h^{-1} (incorporation: 0.5 mol%; M_w: 7.0 kg·mol^{-1}) and AA with an activity of 1.2×10^4 g·mol^{-1}·h^{-1} (incorporation: 0.2 mol%; M_w: 1.2 kg·mol^{-1}), demonstrating that the N-bridge motif strengthens metal–ligand binding (as evidenced by ligand exchange experiments) and promotes polar-monomer insertion.

In addition to structural rigidification, the systematic variation of backbone substituents provides fundamental insights into catalyst behavior. Zhu *et al.* correlated backbone electronics and sterics with the performance of phosphine–carbonyl Pd catalysts (**86**) (Fig. 24).[84] The introduction of an electron-donating isopropyl group (**86d**) strongly suppressed chain transfer, yielding high-M_w copolymers (57.6 kg·mol^{-1}) with 1.8 mol% MA incorporation. Conversely, the methyl-substituted variant **86b** achieved higher incorporation (3.5 mol%) but lower M_w (23.2 kg·mol^{-1}), whereas the cyclic **86i** suffered from reduced M_w (12.2 kg·mol^{-1}). Notably, **86b** proved to be versatile, copolymerizing AA with 3.3 mol% incorporation (activity: 8.0×10^3 g·mol^{-1}·h^{-1}; M_w: 24.4 kg·mol^{-1}) and allyl acetate (ALA) with 1.1 mol% incorporation (activity: 2.5×10^3 g·mol^{-1}·h^{-1}; M_w: 31.5 kg·mol^{-1}), confirming that electron-donating backbone substituents mitigated β-H elimination and enhanced MW.

To optimize the hemilabile phosphine-amide catalysts, Jian

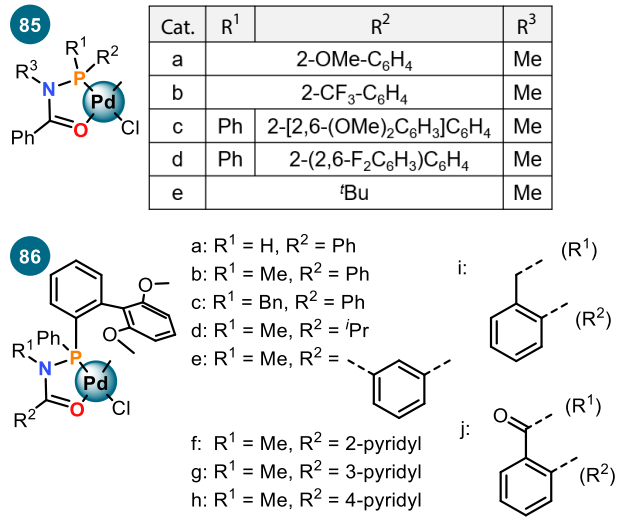

Cat.	R^1	R^2	R^3
a		2-OMe-C_6H_4	Me
b		2-CF_3-C_6H_4	Me
c	Ph	2-[2,6-$(OMe)_2C_6H_3$]C_6H_4	Me
d	Ph	2-(2,6-$F_2C_6H_3$)C_6H_4	Me
e		^{t}Bu	Me

Fig. 24 Phosphine-carbonyl Pd catalysts.

https://doi.org/10.1007/s10118-026-3621-x

et al. employed a cyclization strategy to yield N-bridged Pd catalysts with variable ring sizes (**87**) (Fig. 25).[85] Catalytic performance correlated with ring size; seven-membered **87d** outperformed acyclic analogs, delivering 4.1 mol% MA incorporation with a polymerization activity of 1.5×10^4 g·mol^{-1}·h^{-1} and M_w of 1.3 kg·mol^{-1}. Moreover, catalyst **87d** exhibited broad substrate tolerance, enabling the copolymerization of ethylene with *t*BA (activity: 8.3×10^3 g·mol^{-1}·h^{-1}; incorporation: 4.9 mol%) and AA (activity: 8.0×10^2 g·mol^{-1}·h^{-1}; incorporation: 3.9 mol%), respectively. Mechanistically, the larger ring structure was credited with increasing the N-atom electron density, thereby stabilizing the active species against deactivation.

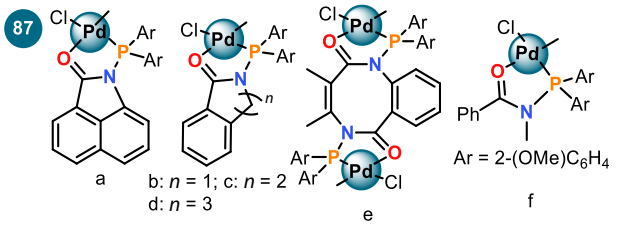

Fig. 25 Other unclassified Pd catalysts.

3.4 Other Unclassified Pd Catalysts

In addition to the widely studied Pd systems described above, several alternative catalysts have been developed to enable the copolymerization of ethylene with fundamental polar monomers. For instance, Cai *et al.* introduced [P,N]-type phosphinobenzenamine Pd catalysts, revealing that increased steric bulk is critical: complex **88b** (%V_{bur}: 51.6%) markedly outperformed the less hindered **88a** (%V_{bur}: 46.9%) by delivering superior thermal stability and high activity at 100 °C (Fig. 26).[180] Nevertheless, MA incorporation remained a challenge: catalyst **88b** reached only 0.1 mol% incorporation (activity: 5.0×10^3 g·mol^{-1}·h^{-1}), and the bulkier **88e** nearly completely suppressed MA insertion. Although tolerance toward long-chain esters (*e.g.*, 5-hexenyl acetate, 1.85% incorporation) was observed, these results suggest that the electronic nature of the [P,N] backbone is generally less favorable for acrylate incorporation than the [P,O] framework.

In addition to phosphine-based ligands, architectures based on strong σ-donating carbon centers have been investigated. Building on the robust imidazo[1,5-a]quinolin-9-olate-1-ylidene (IzQO) platform, a class of neutral, fused N-heterocyclic carbene (NHC)—O chelates known for polar tolerance, Akita and Nozaki appended a methoxyethoxy side chain to enable external regulation (Fig. 26).[181,182] Without additives, catalyst **89** yielded moderate MA incorporation (1.1 mol%), with an M_n of 11.7 kg·mol^{-1}. Addition of $LiBArF_4$ substantially increased copolymerization activity (4.3×10^3 g·mol^{-1}·h^{-1} versus 2.4×10^3 g·mol^{-1}·h^{-1}) and incorporation (1.1 mol% versus 1.3 mol%), but reduced M_n to 1.4 kg·mol^{-1}. Mechanistic studies indicated that Li^+ coordination to the side chain decreased the electron density at the Pd center, accelerating chain transfer, whereas larger cations (Na^+ and Cs^+) or coordinating anions suppressed incorporation.

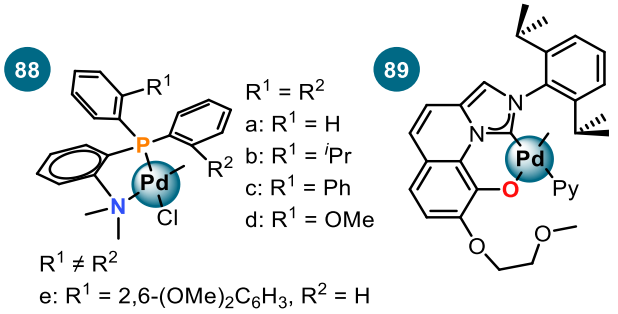

Fig. 26 Other unclassified Pd catalysts.

4 CONCLUSIONS AND OUTLOOK

Substantial progress has been made in the coordination-insertion copolymerization of ethylene with fundamental polar monomers, driven primarily by innovative ligand design strategies for Ni and Pd catalysts. It is now evident that the delicate interplay between steric shielding and electronic perturbation governs chain-transfer rates, β-H elimination propensities, and the coordination of polar monomers, thereby directly dictating polymer MW, topology, and comonomer incorporation. Although Pd-based platforms generally deliver superior insertion selectivity and often the best overall performance, their broader application remains constrained by cost and supply considerations. Conversely, Ni catalysts, benefiting from their lower cost and greater abundance, have witnessed marked gains in thermal stability, impurity tolerance, comonomer incorporation, and achievable MW through backbone rigidification, axial-interaction engineering, and judicious electronic tuning. Notably, phosphine-phenolate and related phosphine-enolate nickel catalysts have advanced across multiple fronts, including robustness, activity, and MW control, positioning them as the most promising candidates for near-term industrial applications (Table 1).

Looking forward, six research thrusts warrant prioritization. First, achieving a deeper mechanistic resolution of the elementary steps is imperative. Integrating high-fidelity DFT and wavefunction methods with microkinetic modeling and machine-learning-assisted screening will enable truly quantitative, predictive ligand design. Second, the widespread adoption of *in situ* and operando spectroscopies (*e.g.*, rapid-scan IR, time-resolved NMR, XAS/XES, and stopped-flow MS) alongside rapid sampling kinetics is essential for capturing active species dynamics and transient intermediates under realistic conditions. Third, catalyst engineering should emphasize modular, tunable frameworks that synergize constrained three-dimensional geometries with adjustable axial interactions, hemilabile sites, and ion-pairing strategies to enhance polar tolerance without sacrificing activity. Fourth, the field urgently requires standardized reporting metrics (including temperature, pressure, concentration, TOF, MW distributions, and chain-transfer rates, *e.g.*, unifying activity units to g·mol^{-1}·h^{-1} versus TOF) to enable rigorous cross-study comparisons and facilitate data-driven discovery. Fifth, the comonomer scope should be expanded to include bio-derived and sustainable polar monomers, accompanied by parallel assessments of feedstock availability, life cycle impacts, and downstream processability. Sixth, industrial translation necessitates that thermal stability at elevated temperatures (*e.g.*, >130 °C for solution processes) and heterogenization strategies to prevent fouling be integrated early in discovery campaigns, ensuring that promising homogeneous systems

Table 1 Overview of copolymerization of ethylene with fundamental polar monomers using Ni and Pd catalysts (2020–2025) [a].

Catalyst precursors	Polar monomers [b]	Activity [c] ($g \cdot mol^{-1} \cdot h^{-1}$)	M_n [c] ($g \cdot mol^{-1}$)	Incorporation (mol%)	Polymer characteristics	Ref.
α-Diimine Ni catalysts	MA, *n*BA	10^3–10^5	10^4–10^6	0.6–5.2	Branched copolymers	[62,63]
Pyridine-imine Ni catalysts	MA	10^2–10^4	10^2–10^4	0.2–35.0	Hyperbranched oils to semi-crystalline solids	[64–66]
	VAc	10^3	10^4	0.3		[66]
	VTES	10^4–10^5	10^4	3.1–5.9		[66]
[N,O] Ni catalysts	MA, *n*BA, *t*BA, HFBA, PA	10^3–10^5	10^3–10^5	0.2–5.4	Branched copolymers	[69–72]
	VTMS	10^4–10^5	10^3–10^4	1.6–10.8		[69,71,72]
	AA, AAm	10^4–10^6	10^3–10^4	0.1–2.6		[73,74]
Bisphosphine monoxide Ni catalysts	MA	10^3–10^4	10^2–10^4	0.3–8.1	Linear copolymers	[80–82]
	VTMS	10^4	10^3	2.4–4.2		[81]
Phosphine-carbonyl Ni catalysts	MA, AIA	10^2–10^4	10^2–10^4	0.7–4.4	Lightly branched copolymers	[83–85]
	BVE	10^2	10^3	2.0–2.6		[83]
Phosphine-phenolate Ni catalysts	MA, *n*BA, *t*BA, AIA	10^4–10^8	10^4–10^6	0.3–8.2	Linear copolymers	[75,96–112]
	VTMS	10^4	10^5	0.1		[99]
	DMI	10^3–10^4	10^3–10^4	0.4–1.8		[96]
Phosphine-enolate Ni catalysts	*t*BA	10^5–10^7	10^3–10^4	0.4–3.5	Linear copolymers	[107,113]
α-Diimine Pd catalysts	MA	10^2–10^4	10^3–10^5	0.2–20.7	Highly branched copolymers	[40,125–146]
	AA	10^3–10^4	10^4	0.7–2.1		[125,135]
Pyridine-imine Pd catalysts	MA	10^2–10^4	10^2–10^4	1.0–23.7	Hyperbranched oils to high-MW copolymers	[147–158]
Amine-imine Pd catalysts	MA	10^3	10^3–10^4	0.8–3.2	Branched copolymers	[165]
Phosphine–sulfonate Pd catalysts	MA, *n*BA, EGMA, AAEA,	10^3–10^6	10^4–10^5	0.2–13.0	Linear copolymers	[172,175]
	AA	10^3–10^4	10^3–10^4	4.1–8.3		[172,173]
Bisphosphine monoxide Pd catalysts	MA	10^4–10^5	10^3–10^4	0.3–7.1	Linear copolymers	[81,177–179]
	VAc	10^3	10^3	0.3		[178]
	BVE	10^4	10^3	0.3–0.4		[178,179]
	VTMS	10^3	10^3	2.1		[177]
	AA, AN	10^3–10^4	10^2–10^3	0.3–6.2		[177–179]
Phosphine-carbonyl Pd catalysts	MA, *t*BA, AIA	10^3–10^4	10^2–10^4	0.7–4.9	Linear copolymers	[83–85]
	BVE	10^4	10^3	0.5		[83]
	AA	10^2–10^4	10^3–10^4	0.2–3.9		[83–85]

[a] Selected data from the representative systems discussed in this feature article. [b] Monomers are classified as acrylates, VAc, BVE, vinylsilanes, and AA/AN, according to the type of polar group and the difficulty of copolymerization. [c] The activities and molecular weights should only be taken as a measure of the order of magnitude.

can be transformed into robust and reactor-compatible forms. Notably, very recently we have developed an innovative neutral N^O-type *α*-ketocarboxamide nickel catalyst platform and proposed the high-temperature solution polymerization method for the synthesis of ethylene-acrylate copolymers. Owing to the exceptional thermostability (150 °C) of the *α*-ketocarboxamide nickel catalyst, at the industrially preferred 110–150 °C, ethylene-acrylate copolymers with high molecular weights of 103–627 kDa were obtained.[183]

In summary, the path ahead calls for tighter integration of computation, mechanistic spectroscopy, and practical catalyst engineering. By coupling parametric ligand design with standardized metrics and application-aware testing, the community can realistically move from landmark laboratory demonstrations to commercially viable routes for functionalized polyolefins.

BIOGRAPHY

2026 Rising Scholar: Zhong-bao Jian is a full professor at the Changchun Institute of Applied Chemistry (CIAC), Chinese Academy of Sciences since 2017. He obtained his PhD at CIAC in 2013. He then became an Alexander von Humboldt Fellow and did postdoctoral researches at the University of Konstanz, Germany (2013–2015), and at the University of Münster, Germany (2015–2017). His current research interests at CIAC include olefin polymerization, polyolefin synthesis, optical polyolefin and sustainable polyolefin. He has published > 100 papers and authorized > 20 patents.

Conflict of Interests

The authors declare no interest conflict.

ACKNOWLEDGMENTS

This work was financially supported by the National Natural Science Foundation of China (Nos. U23B6011, 22501275), and the Jilin Provincial Science and Technology Department Program (No. 20250102080JC).

REFERENCES

1 Hustad, P. D. Frontiers in olefin polymerization: reinventing the world's most common synthetic polymers. *Science* **2009**, *325*, 704–707.

Graphical Abstract

Recent Advances in Nickel- and Palladium-catalyzed Copolymerization of Ethylene with Fundamental Polar Monomers

Kang-Kang Li and Zhong-Bao Jian

Changchun Institute of Applied Chemistry, Chinese Academy of Sciences

This feature surveys 2020–present Ni/Pd catalysts for ethylene copolymerization with fundamental polar monomers, linking [N,N], [N,O], and [P,O] ligand platforms to mechanisms, microstructure, and scale-up priorities.

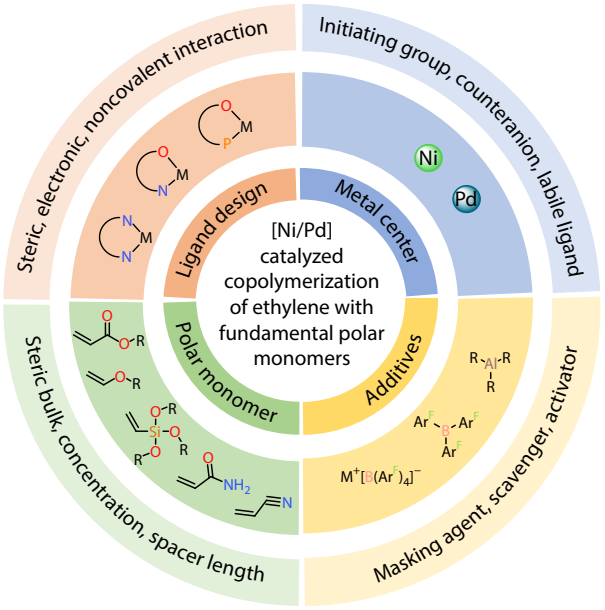

Chinese J. Polym. Sci. 2026, 44, 2062–2085 *https://doi.org/10.1007/s10118-026-3621-x*

2 Stürzel, M.; Mihan, S.; Mülhaupt, R. From multisite polymerization catalysis to sustainable materials and all-polyolefin composites. *Chem. Rev.* **2016**, *116*, 1398–1433.
3 Jubinville, D.; Esmizadeh, E.; Saikrishnan, S.; Tzoganakis, C.; Mekonnen, T. A comprehensive review of global production and recycling methods of polyolefin (PO) based products and their post-recycling applications. *Sustain. Mater. Technol.* **2020**, *25*, e00188.
4 Keyes, A.; Basbug Alhan, H. E.; Ordonez, E.; Ha, U.; Beezer, D. B.; Dau, H.; Liu, Y.; Tsogtgerel, E.; Jones, G. R.; Harth, E. Olefins and vinyl polar monomers: bridging the gap for next generation materials. *Angew. Chem. Int. Ed.* **2019**, *58*, 12370–12391.
5 Mu, H.; Jian, Z. Stereoselective copolymerization of olefin with polar monomers to access stereoregular functionalized polyolefins. *Org. Mater.* **2022**, *4*, 178–189.
6 Yu, Y.; Zhao, B.; Jiao, N. Recent advances in the chemical transformation of polyolefins into small molecules. *Acta Polymerica Sinica* (in Chinese) **2026**, *57*, 305–338.
7 Zhou, G.; Cui, L.; Mu, H.; Jian, Z. Custom-made polar monomers utilized in nickel and palladium promoted olefin copolymerization. *Polym. Chem.* **2021**, *12*, 3878–3892.
8 Tan, C.; Chen, M.; Zou, C.; Chen, C. Potentially practical catalytic systems for olefin-polar monomer coordination copolymerization. *CCS Chem.* **2023**, *6*, 882–897.
9 Tan, C.; Si, G.; Zou, C.; Chen, C. Functional polyolefins and composites. *Angew. Chem. Int. Ed.* **2025**, *64*, e202424529.
10 Boaen, N. K.; Hillmyer, M. A. Post-polymerization functionalization of polyolefins. *Chem. Soc. Rev.* **2005**, *34*, 267–275.
11 Franssen, N.; Reek, J.; de Bruin, B. Synthesis of functional 'polyolefins': state of the art and remaining challenges. *Chem. Soc. Rev.* **2013**, *42*, 5809–5832.
12 Plummer, C.; Li, L.; Chen, Y. The post-modification of polyolefins with emerging synthetic methods. *Polym. Chem.* **2020**, *11*, 6862–6872.
13 Balzade, Z.; Sharif, F.; Ghaffarian Anbaran, S. R. Tailor-made functional polyolefins of complex architectures: Recent advances, applications, and prospects. *Macromolecules* **2022**, *55*, 6938–6972.
14 Baffie, F.; Sinniger, L.; Lansalot, M.; Monteil, V.; D'Agosto, F. From radical to reversible-deactivation radical polymerization of ethylene. *Prog. Polym. Sci.* **2025**, *162*, 101932.
15 Tan, C.; Chen, C. Emerging palladium and nickel catalysts for copolymerization of olefins with polar monomers. *Angew. Chem. Int. Ed.* **2019**, *58*, 7192–7200.
16 Dong, J.; Hu, Y. Design and synthesis of structurally well-defined functional polyolefins via transition metal-mediated olefin polymerization chemistry. *Coord. Chem. Rev.* **2006**, *250*, 47–65.
17 Chen, Z.; Brookhart, M. Exploring ethylene/polar vinyl monomer copolymerizations using Ni and Pd *α*-diimine catalysts. *Acc. Chem. Res.* **2018**, *51*, 1831–1839.
18 Luckham, S.; Nozaki, K. Toward the copolymerization of propylene with polar comonomers. *Acc. Chem. Res.* **2021**, *54*, 344–355.
19 Ittel, S.; Johnson, L.; Brookhart, M. Late-metal catalysts for ethylene homo- and copolymerization. *Chem. Rev.* **2000**, *100*, 1169–1203.
20 Chen, C. Designing catalysts for olefin polymerization and copolymerization: Beyond electronic and steric tuning. *Nat. Rev. Chem.* **2018**, *2*, 6–14.

21 Baier, M. C.; Zuideveld, M. A.; Mecking, S. Post-metallocenes in the industrial production of polyolefins. *Angew. Chem. Int. Ed.* **2014**, *53*, 9722–9744.
22 Cui, D. Studies on homo- and co-polymerizations of polar and non-polar monomers using rare-earth metal catalysts. *Acta Polymerica Sinica* (in Chinese) **2020**, *51*, 12–29.
23 Fan, X. Z.; Luo, S. F.; Zhang, Y. J.; Gao, W. X.; He, A. H. Research progress on supported Ziegler-Natta catalysts—activation of $MgCl_2$ support and its influences on olefin polymerizations. *Polym. Bull.* (in Chinese) **2024**, *37*, 1414–1427.
24 Li, C.; Fan, G.; Zheng, G.; Gao, R.; Liu, L. Groups 3 and 4 single-site catalysts for olefin-polar monomer copolymerization. *Chin. Chem. Lett.* **2025**, *36*, 111297.
25 Li, Q.; Guo, Z.; Li, X.; Chen, J.; Qu, S.; Wei, Y.; Wen, Z.; Wang, W. Copolymerization of ethylene with polar monomers by group 4 catalysts. *Polym. Rev.* **2025**, *65*, 365–424.
26 Nakamura, A.; Ito, S.; Nozaki, K. Coordination–insertion copolymerization of fundamental polar monomers. *Chem. Rev.* **2009**, *109*, 5215–5244.
27 Mitchell, N. E.; Long, B. K. Recent advances in thermally robust, late transition metal-catalyzed olefin polymerization. *Polym. Int.* **2019**, *68*, 14–26.
28 Li, Y.; Wang, F.; Cao, Y. Late transition metal complexes for olefin copolymerization with polar monomers. *Chin. J. Org. Chem.* **2021**, *41*, 1396–1433.
29 Wu, R.; Wu, W.; Stieglitz, L.; Gaan, S.; Rieger, B.; Heuberger, M. Recent advances on *α*-diimine Ni and Pd complexes for catalyzed ethylene (co)polymerization: a comprehensive review. *Coord. Chem. Rev.* **2023**, *474*, 214844.
30 Xing, Y.; Liu, S.; Li, Z. Recent progress in dinuclear transition metal catalysts for olefin polymerization. *Macromol. Rapid Commun.* **2025**, *46*, e2500091.
31 Johnson, L. K.; Killian, C. M.; Brookhart, M. New Pd(II)- and Ni(II)-based catalysts for polymerization of ethylene and *α*-olefins. *J. Am. Chem. Soc.* **1995**, *117*, 6414–6415.
32 Johnson, L. K.; Mecking, S.; Brookhart, M. Copolymerization of ethylene and propylene with functionalized vinyl monomers by palladium(II) catalysts. *J. Am. Chem. Soc.* **1996**, *118*, 267–268.
33 Guan, Z.; Cotts, P. M.; McCord, E. F.; McLain, S. J. Chain walking: a new strategy to control polymer topology. *Science* **1999**, *283*, 2059–2062.
34 Camacho, D. H.; Salo, E. V.; Ziller, J. W.; Guan, Z. Cyclophane-based highly active late-transition-metal catalysts for ethylene polymerization. *Angew. Chem. Int. Ed.* **2004**, *43*, 1821–1825.
35 Meinhard, D.; Wegner, M.; Kipiani, G.; Hearley, A.; Reuter, P.; Fischer, S.; Marti, O.; Rieger, B. New nickel(II) diimine complexes and the control of polyethylene microstructure by catalyst design. *J. Am. Chem. Soc.* **2007**, *129*, 9182–9191.
36 Rhinehart, J. L.; Brown, L. A.; Long, B. K. A robust Ni(II) *α*-diimine catalyst for high temperature ethylene polymerization. *J. Am. Chem. Soc.* **2013**, *135*, 16316–16319.
37 Takano, S.; Takeuchi, D.; Osakada, K.; Akamatsu, N.; Shishido, A. Dipalladium catalyst for olefin polymerization: introduction of acrylate units into the main chain of branched polyethylene. *Angew. Chem. Int. Ed.* **2014**, *53*, 9246–9250.
38 Allen, K.; Campos, J.; Daugulis, O.; Brookhart, M. Living polymerization of ethylene and copolymerization of ethylene/methyl acrylate using "sandwich" diimine palladium catalysts. *ACS Catal.* **2015**, *5*, 456–464.
39 Dai, S.; Sui, X.; Chen, C. Highly robust palladium(II) *α*-diimine catalysts for slow-chain-walking polymerization of ethylene and copolymerization with methyl acrylate. *Angew. Chem. Int. Ed.* **2015**, *54*, 9948–9953.
40 Zhang, Y.; Wang, C.; Mecking, S.; Jian, Z. Ultrahigh branching of main-chain-functionalized polyethylenes by inverted insertion selectivity. *Angew. Chem. Int. Ed.* **2020**, *59*, 14296–14302.
41 Drent, E.; van Dijk, R.; van Ginkel, R.; van Oort, B.; Pugh, R. Palladium catalysed copolymerisation of ethene with alkylacrylates: polar comonomer built into the linear polymer chain. *Chem. Commun*. **2002**, 744–745.
42 Skupov, K. M.; Piche, L.; Claverie, J. P. Linear polyethylene with tunable surface properties by catalytic copolymerization of ethylene with *N*-Vinyl-2-pyrrolidinone and *N*-Isopropylacrylamide. *Macromolecules* **2008**, *41*, 2309–2310.
43 Ravasio, A.; Boggioni, L.; Tritto, I. Copolymerization of ethylene with norbornene by neutral aryl phosphine sulfonate palladium catalyst. *Macromolecules* **2011**, *44*, 4180–4186.
44 Friedberger, T.; Wucher, P.; Mecking, S. Mechanistic insights into polar monomer insertion polymerization from acrylamides. *J. Am. Chem. Soc.* **2012**, *134*, 1010–1018.
45 Chen, M.; Chen, C. Rational design of high-performance phosphine sulfonate nickel catalysts for ethylene polymerization and copolymerization with polar monomers. *ACS Catal.* **2017**, *7*, 1308–1312.
46 Li, K.; Cui, L.; Zhang, Y.; Jian, Z. Amide-functionalized polyolefins and facile post-transformations. *Macromolecules* **2023**, *56*, 915–922.
47 Li, K.; Jian, Z. Switchable polyolefins from polar functionalization to degradability. *CCS Chem.* **2024**, *6*, 1941–1950.
48 Li, K.; Cui, L.; Zhang, Y.; Jian, Z. Synthesis and chemical transformation of nitrogen-rich polyolefins through copolymerization of ethylene with polar cyclic olefins. *Macromolecules* **2025**, *58*, 9412–9419.
49 Mu, H.; Pan, L.; Song, D.; Li, Y. Neutral nickel catalysts for olefin homo- and copolymerization: relationships between catalyst structures and catalytic properties. *Chem. Rev.* **2015**, *115*, 12091–12137.
50 Zhang, Y.; Mu, H.; Pan, L.; Wang, X.; Li, Y. Robust bulky [P,O] neutral nickel catalysts for copolymerization of ethylene with polar vinyl monomers. *ACS Catal.* **2018**, *8*, 5963–5976.
51 Li, J.; Liu, Y.; Mu, H.; Jian, Z. Mono- and bi-nuclear phosphine-phenolate neutral nickel catalysts *via* simple schiff-base condensation for ethylene polymerization. *J. Catal.* **2024**, *432*, 115413.
52 Huang, X.; Zheng, J.; Zhou, J.; Wu, Y.; Wang, J.; Raza, S.; Liu, P.; Wang, W.; Shi, S. Recent advances in transition metal-catalyzed ethylene/polar olefin copolymerization. *Coord. Chem. Rev.* **2026**, *548*, 217147.
53 Wang, C.; Friedrich, S.; Younkin, T. R.; Li, R. T.; Grubbs, R. H.; Bansleben, D. A.; Day, M. W. Neutral nickel(II)-based catalysts for ethylene polymerization. *Organometallics* **1998**, *17*, 3149–3151.
54 Younkin, T.; Conner, E.; Henderson, J.; Friedrich, S.; Grubbs, R.; Bansleben, D. Neutral, single-component nickel(II) polyolefin catalysts that tolerate heteroatoms. *Science* **2000**, *287*, 460–462.
55 Zhang, R.; Gao, R.; Gou, Q.; Lai, J.; Li, X. Recent advances in the copolymerization of ethylene with polar comonomers by nickel catalysts. *Polymers* **2022**, *14*, 3809.
56 Zheng, H.; Qiu, Z.; Li, D.; Pei, L.; Gao, H. Advance on nickel- and palladium-catalyzed insertion copolymerization of ethylene and acrylate monomers. *J. Polym. Sci.* **2023**, *61*, 2987–3021.
57 Wang, Y.; Lai, J.; Gao, R.; Gou, Q.; Li, B.; Zheng, G.; Zhang, R.; Yue, Q.; Song, Z.; Guo, Z. Recent advances in nickel catalysts with industrial exploitability for copolymerization of ethylene with polar monomers. *Polymers* **2024**, *16*, 1676.
58 Mu, H.; Zhou, G.; Hu, X.; Jian, Z. Recent advances in nickel mediated copolymerization of olefin with polar monomers. *Coord. Chem. Rev.* **2021**, *435*, 213802.
59 Chen, M.; Chen, C. The synthesis of functionalized polyolefin

materials and research on material properties. *Polym. Bull.* (in Chinese) **2021**, *34*, 26−34.
60 Zhang, Y.; Zhang, Y.; Hu, X.; Wang, C.; Jian, Z. Advances on controlled chain walking and suppression of chain transfer in catalytic olefin polymerization. *ACS Catal.* **2022**, *12*, 14304−14320.
61 Zheng, H.; Gao, H. Noncovalent interactions in late transition metal-catalyzed polymerization of olefins. *Macromolecules* **2024**, *57*, 6899−6913.
62 Zheng, H.; Qiu, Z.; Gao, H.; Li, D.; Cheng, Z.; Tu, G.; Gao, H. Noncovalent Ni-phenyl interactions promoted *α*-diimine nickel-catalyzed copolymerization of ethylene and methyl acrylate. *Macromolecules* **2024**, *57*, 5279−5288.
63 Wang, X.; Ma, L.; Dong, B.; Zhang, C.; Zhang, X.; Liu, H. Axial anagostic interaction in *α*-diimine nickel catalysts: An ultraefficient occupation strategy in suppressing associative chain transfers to achieve UHMWPEs. *Macromolecules* **2025**, *58*, 1888−1897.
64 Saki, Z.; D'Auria, I.; Dall'Anese, A.; Milani, B.; Pellecchia, C. Copolymerization of ethylene and methyl acrylate by pyridylimino Ni(II) catalysts affording hyperbranched poly(ethylene-co-methyl acrylate)s with tunable structures of the ester groups. *Macromolecules* **2020**, *53*, 9294−9305.
65 D'Auria, I.; Saki, Z.; Liu, M.; Sun, W.; Pellecchia, C. Copolymerization of ethylene and methyl acrylate by dibenzocycloheptyl-substituted aryliminopyridyl Ni(II) catalysts. *Macromolecules* **2022**, *2*, 500−508.
66 Rauf, H.; Liu, Y.; Arslan, M.; Solanki, S.; Deydier, E.; Poli, R.; Grabow, L.; Harth, E. Benchtop-stable carbyl iminopyridyl Ni^{II} complexes for olefin polymerization. *ACS Catal.* **2024**, *14*, 13136−13147.
67 Schnitte, M.; Scholliers, J. S.; Riedmiller, K.; Mecking, S. Remote perfluoroalkyl substituents are key to living aqueous ethylene polymerization. *Angew. Chem. Int. Ed.* **2020**, *59*, 3258−3263.
68 Mecking, S.; Schnitte, M. Neutral nickel(II) catalysts: From hyperbranched oligomers to nanocrystal-based materials. *Acc. Chem. Res.* **2020**, *53*, 2738−2752.
69 Liang, T.; Goudari, S. B.; Chen, C. A simple and versatile nickel platform for the generation of branched high molecular weight polyolefins. *Nat. Commun.* **2020**, *11*, 372.
70 Cui, L.; Hu, X.; Zhang, Y.; Jian, Z. Systematic study of fluorine effect on *α*-ketiminato nickel catalyzed ethylene (co)polymerization. *Acta Polymerica Sinica* (in Chinese) **2021**, *52*, 531−540.
71 Tian, W.; Kong, X.; Dai, S.; Xie, J.; Chen, Q.; Liu, Z.; Zhang, S.; Wang, F. Synthesis of methyl-branched functionalized polyethylene using *α*-imino ketone nickel catalysts for high-temperature ethylene (co)polymerization. *ACS Appl. Polym. Mater.* **2025**, *7*, 16228−16240.
72 Nan, C.; Pang, T.; Zhao, J.; Fan, L.; Zou, C.; Hao, X.; Song, M.; Gong, J.; Chen, C.; Jiang, H. Novel photoresponsive dinuclear nickel catalysts for ethylene (co)polymerization. *Sci. China Chem.* **2025**, *68*, 714−722.
73 Ji, G.; Chen, Z.; Wang, X.; Ning, X.; Xu, C.; Zhang, X.; Tao, W.; Li, J.; Gao, Y.; Shen, Q.; Sun, X.; Wang, H.; Zhao, J.; Zhang, B.; Guo, Y.; Zhao, Y.; Sun, J.; Luo, Y.; Tang, Y. Direct copolymerization of ethylene with protic comonomers enabled by multinuclear Ni catalysts. *Nat. Commun.* **2021**, *12*, 6283.
74 Yu, S. Y.; Wang, X. Y.; Sun, X. L.; Gao, Y.; Zhao, Y.; Ning, X. S.; Ji, G.; Lu, Y.; Yang, J.; Liu, Z. P.; Tang, Y. Cyano-functionalized polyethylenes from ethylene/acrylamide copolymerization. *Nat. Commun.* **2025**, *16*, 2461.
75 Xiong, S.; Hong, A.; Ghana, P.; Bailey, B. C.; Spinney, H. A.; Bailey, H.; Henderson, B. S.; Marshall, S.; Agapie, T. Acrylate-induced *β*-H elimination in coordination insertion copolymerization catalyzed by nickel. *J. Am. Chem. Soc.* **2023**, *145*, 26463−26471.
76 Carrow, B. P.; Nozaki, K. Synthesis of functional polyolefins using cationic bisphosphine monoxide–palladium complexes. *J. Am. Chem. Soc.* **2012**, *134*, 8802−8805.
77 Mitsushige, Y.; Yasuda, H.; Carrow, B.; Ito, S.; Kobayashi, M.; Tayano, T.; Watanabe, Y.; Okuno, Y.; Hayashi, S.; Kuroda, J.; Okumura, Y.; Nozaki, K. Methylene-bridged bisphosphine monoxide ligands for palladium-catalyzed copolymerization of ethylene and polar monomers. *ACS Macro Lett.* **2018**, *7*, 305−311.
78 Chen, M.; Chen, C. A versatile ligand platform for palladium- and nickel-catalyzed ethylene copolymerization with polar monomers. *Angew. Chem. Int. Ed.* **2018**, *57*, 3094−3098.
79 Jung, J.; Yasuda, H.; Nozaki, K. Copolymerization of nonpolar olefins and allyl acetate using nickel catalysts bearing a methylene-bridged bisphosphine monoxide ligand. *Macromolecules* **2020**, *53*, 2547−2556.
80 Xu, M.; Yu, F.; Li, P.; Xu, G.; Zhang, S.; Wang, F. Enhancing chain initiation efficiency in the cationic allyl-nickel catalyzed (co)polymerization of ethylene and methyl acrylate. *Inorg. Chem.* **2020**, *59*, 4475−4482.
81 Zou, C.; Liao, D.; Pang, W.; Chen, M.; Tan, C. Versatile PNPO ligands for palladium and nickel catalyzed ethylene polymerization and copolymerization with polar monomers. *J. Catal.* **2021**, *393*, 281−289.
82 Tahmouresilerd, B.; Xiao, D.; Do, L. Rigidifying cation-tunable nickel catalysts increases activity and polar monomer incorporation in ethylene and methyl acrylate copolymerization. *Inorg. Chem.* **2021**, *60*, 19035−19043.
83 Cui, L.; Jian, Z. A N-bridged strategy enables hemilabile phosphine-carbonyl palladium and nickel catalysts to mediate ethylene polymerization and copolymerization with polar vinyl monomers. *Polym. Chem.* **2020**, *11*, 6187−6193.
84 Zhu, N.; Liang, T.; Huang, Y.; Pang, W.; Chen, M.; Tan, C. Influences of ligand backbone substituents on phosphinecarbonylpalladium and -nickel catalysts for ethylene polymerization and copolymerization with polar monomers. *Inorg. Chem.* **2021**, *60*, 13080−13090.
85 Cui, L.; Chu, Y.; Liu, D.; Han, Y.; Mu, H.; Jian, Z. Enhancement on hemilabile phosphine-amide palladium and nickel catalysts for ethylene (co)polymerization with polar monomers using a cyclizing strategy. *Chinese J. Polym. Sci.* **2022**, *40*, 241−247.
86 Keim, W. Oligomerization of ethylene to *α*-olefins: discovery and development of the Shell Higher Olefin Process (SHOP). *Angew. Chem. Int. Ed.* **2013**, *52*, 12492−12496.
87 Li, J.; Zhang, J.; Jian, Z. Recent advances in phosphine-phenolate neutral nickel catalyzed olefin polymerization and copolymerization with polar monomers. *Polym. Bull.* (in Chinese) **2023**, *36*, 657−668.
88 Klabunde, U.; Ittel, S. Nickel catalysis for ethylene homopolymerization and co-polymerization. *J. Mol. Catal.* **1987**, *41*, 123−134.
89 Gibson, V.; Tomov, A. Functionalised polyolefin synthesis using [P,O]Ni catalysts. *Chem. Commun*. **2001**, 1964-1965.
90 Guo, C.; Peulecke, N.; Basvani, K.; Kinderman, M.; Heinicke, J. 2-phosphinophenolate nickel catalysts: formation of ethylene copolymers with isolated *sec*-alkyl, aryl, and functionally substituted alkyl groups. *Macromolecules* **2010**, *43*, 1416-1424.
91 Zhang, Y.; Li, W.; Li, B.; Mu, H.; Li, Y. Well-defined phosphino-phenolate neutral nickel(II) catalysts for efficient (co)polymerization of norbornene and ethylene. *Dalton Trans.* **2015**, *44*, 7382−7394.
92 Mu, H.; Li, Y.; Li, Y. Ethylene homo-and copolymerization by single component phosphinophenolate neutral nickel catalysts. *Chin. J. Org. Chem.* **2012**, *29*, 1381−1388.

93 Xin, B.; Sato, N.; Tanna, A.; Oishi, Y.; Konishi, Y.; Shimizu, F. Nickel catalyzed copolymerization of ethylene and alkyl acrylates. *J. Am. Chem. Soc.* **2017**, *139*, 3611–3614.

94 Lin, F.; Voccia, M.; Odenwald, L.; Göttker-Schnetmann, I.; Falivene, L.; Caporaso, L.; Mecking, S. Origin of suppressed chain transfer in phosphinephenolato Ni(II)-catalyzed ethylene polymerization. *J. Am. Chem. Soc.* **2023**, *145*, 27950–27957.

95 Zhang, Y.; Mu, H.; Wang, X.; Pan, L.; Li, Y. Elaborate tuning in ligand makes a big difference in catalytic performance: Bulky nickel catalysts for (co)polymerization of ethylene with promising vinyl polar monomers. *ChemCatChem* **2019**, *11*, 2329–2340.

96 Wang, X.; Zhang, Y.; Wang, F.; Pan, L.; Wang, B.; Li, Y. Robust and reactive neutral nickel catalysts for ethylene polymerization and copolymerization with a challenging 1,1-disubstituted difunctional polar monomer. *ACS Catal.* **2021**, *11*, 2902–2911.

97 Wang, F.; Pan, L.; Tuskaev, V. A.; Gagieva, S. C.; Li, Y. Phosphine/benzocyclone-based neutral nickel catalysts for ethylene polymerization and copolymerization with polar monomers. *Chinese J. Polym. Sci.* **2024**, *42*, 202–212.

98 Wang, F.; Wang, X.; Pan, L.; Wang, B.; Li, Y. Efficient copolymerization of ethylene with polar divinyl monomer by phosphino-phenolate nickel catalyst. *Chin. J. Chem.* **2023**, *41*, 1037–1044.

99 Peng, D.; He, H.; Pang, W.; Behzadi, S.; Qasim, M. Synthesis of UHMWPE by neutral phosphine-phenolate based nickel catalysts. *Polymer* **2023**, *280*, 126019.

100 Xie, Y.; Yang, F.; Miao, Q.; Zhang, Z.; Wang, W.; Wang, F.; Zou, C. Electronic effect regulated ethylene polymerization and copolymerization of phosphorus phenol nickel catalysts. *Appl. Organomet. Chem.* **2024**, *38*, e7469.

101 Wang, W.; Nie, N.; Xu, M.; Zou, C. Lewis acid modulation in phosphorus phenol nickel catalyzed ethylene polymerization and copolymerization. *Polym. Chem.* **2023**, *14*, 4933–4939.

102 Tian, W.; Guan, H.; Wang, W.; Kong, X.; Pang, W.; Wang, Q.; Wang, F.; Zou, C. Nickel catalyst with excellent thermal stability for ethylene polymerization and copolymerization. *Appl. Organomet. Chem.* **2025**, *39*, e70063.

103 Yang, Q.; Kang, X.; Liu, Y.; Mu, H.; Jian, Z. Ultrahigh molecular weight ethylene-acrylate copolymers synthesized with highly active neutral nickel catalysts. *Angew. Chem. Int. Ed.* **2025**, *64*, e202421904.

104 Liu, Y.; Wang, C.; Mu, H.; Jian, Z. Aqueous coordination-insertion copolymerization for producing high molecular weight polar polyolefins. *Angew. Chem. Int. Ed.* **2024**, *63*, e202404392.

105 Xiong, S.; Shoshani, M.; Zhang, X.; Spinney, H.; Nett, A.; Henderson, B.; Miller, T.; Agapie, T. Efficient copolymerization of acrylate and ethylene with neutral P,O-chelated nickel catalysts: Mechanistic investigations of monomer insertion and chelate formation. *J. Am. Chem. Soc.* **2021**, *143*, 6516–6527.

106 Xiong, S. Y.; Shoshani, M. M.; Nett, A. J.; Spinney, H. A.; Henderson, B. S.; Agapie, T. Nickel-based heterometallic catalysts for ethylene-acrylate copolymerization: Interrogating effects of secondary metal additives. *Organometallics* **2023**, *42*, 2849–2855.

107 Xiong, S.; Ghana, P.; Bailey, B.; Spinney, H.; Henderson, B.; Espinosa, M.; Agapie, T. Impact of labile ligands on catalyst initiation and chain propagation in Ni-catalyzed ethylene/acrylate copolymerization. *ACS Catal.* **2023**, *13*, 5000–5006.

108 Xiong, S. Y.; Spinney, H. A.; Bailey, B. C.; Henderson, B. S.; Tekpor, A. A.; Espinosa, M. R.; Saha, P.; Agapie, T. Switchable synthesis of ethylene/acrylate copolymers by a dinickel catalyst: Evidence for chain growth on both nickel centers and concepts of cation exchange polymerization. *ACS Catal.* **2024**, *14*, 5260–5268.

109 Pineda-Knauseder, A. J.; Woods, T. J.; Guironnet, D. Mono- and trinuclear phosphine-phenolate nickel(II) complexes as precatalysts in ethylene/acrylate copolymerization. *Organometallics* **2025**, *44*, 560–567.

110 Ghana, P.; Xiong, S.; Tekpor, A.; Bailey, B. C.; Spinney, H. A.; Henderson, B. S.; Agapie, T. Catalyst editing *via* post-synthetic functionalization by phosphonium generation and anion exchange for nickel-catalyzed ethylene/acrylate copolymerization. *J. Am. Chem. Soc.* **2024**, *146*, 18797–18803.

111 Zou, C.; Si, G.; Chen, C. A general strategy for heterogenizing olefin polymerization catalysts and the synthesis of polyolefins and composites. *Nat. Commun.* **2022**, *13*, 1954.

112 Zou, C.; Wang, Q.; Si, G.; Chen, C. A co-anchoring strategy for the synthesis of polar bimodal polyethylene. *Nat. Commun.* **2023**, *14*, 1442.

113 Xiong, S.; Hong, A.; Bailey, B. C.; Spinney, H. A.; Senecal, T. D.; Bailey, H.; Agapie, T. Highly active and thermally robust nickel enolate catalysts for the synthesis of ethylene-acrylate copolymers. *Angew. Chem. Int. Ed.* **2022**, *61*, e202206637.

114 Cao, L.; Cai, Z.; Li, M. Phosphinobenzenamine nickel catalyzed efficient copolymerization of methyl acrylate with ethylene and norbornene. *Macromolecules* **2022**, *55*, 3513–3521.

115 Rivet, J.; Henderson, B.; Marshall, S.; Cade, K.; Wilson, D.; Spinney, H.; Hou, J.; Nett, A. Phosphine-imidate-supported nickel catalysts for ethylene/acrylate copolymerization. *Organometallics* **2024**, *43*, 859–865.

116 Du, W.; Zheng, H.; Li, Y.; Cheung, C.; Li, D.; Gao, H.; Deng, H.; Gao, H. Neutral tridentate *α*-sulfonyl-*β*-diimine nickel catalyst for (co)polymerizations of ethylene and acrylates. *Macromolecules* **2022**, *55*, 3096–3105.

117 Li, D.; Qiu, Z.; Xiao, X.; Gao, H.; Feng, C.; Zheng, H.; Gao, H. Effects of ancillary ligands on molecular structure and catalytic properties of tridentate *α*-sulfonate-*β*-diimine nickel complexes toward ethylene (co)polymerization. *Molecular Catalysis* **2025**, *580*, 115136.

118 Chen, J.; Gao, Y.; Marks, T. J. Early transition metal catalysis for olefin–polar monomer copolymerization. *Angew. Chem. Int. Ed.* **2020**, *59*, 14726–14735.

119 Zhao, Y.; Zhang, Z.; Luo, Y. DFT modeling of coordination polymerization of polar olefin monomers by molecular metal complexes. *Inorganics* **2024**, *12*, 233.

120 Liang, D.; Jiang, Y.; Li, S.; Cui, D. Copolymerization of ethylene and polar vinyl monomers by rare-earth metal catalysts. *Acta Polymerica Sinica* (in Chinese) **2024**, *55*, 1487–1494.

121 Tempel, D.; Johnson, L.; Huff, R.; White, P.; Brookhart, M. Mechanistic studies of Pd(II)-*α*-diimine-catalyzed olefin polymerizations. *J. Am. Chem. Soc.* **2000**, *122*, 6686–6700.

122 Wang, C.; Feng, T.; Fu, Z. *α*-diimine nickel catalyst and olefin polymerization—supplementary suggestions for the "coordination polymerization" section in the "polymer chemistry" textbook. *Polym. Bull. (in Chinese)* **2025**, *38*, 137-145.

123 Tran, Q. H.; Brookhart, M.; Daugulis, O. New neutral nickel and palladium sandwich catalysts: Synthesis of ultra-high molecular weight polyethylene (UHMWPE) *via* highly controlled polymerization and mechanistic studies of chain propagation. *J. Am. Chem. Soc.* **2020**, *142*, 7198–7206.

124 Wang, F.; Chen, C. A continuing legend: the Brookhart-type *α*-diimine nickel and palladium catalysts. *Polym. Chem.* **2019**, *10*, 2354–2369.

125 Muhammad, Q.; Tan, C.; Chen, C. Concerted steric and electronic effects on *α*-diimine nickel- and palladium-catalyzed ethylene polymerization and copolymerization. *Sci. Bull.* **2020**, *65*, 300–307.

126 Wang, G.; Peng, D.; Sun, Y.; Chen, C. Interplay of supramolecular chemistry and photochemistry with palladium-catalyzed

ethylene polymerization. *CCS Chem.* **2020**, *2*, 2025–2034.
127 Zhang, Y.; Jian, Z. Polar additive triggered branching switch and block polyolefin topology in living ethylene polymerization. *Macromolecules* **2021**, *54*, 3191–3196.
128 Alberoni, C.; D'Alterio, M. C.; Balducci, G.; Immirzi, B.; Polentarutti, M.; Pellecchia, C.; Milani, B. Tunable "in-chain" and "at the end of the branches" methyl acrylate incorporation in the polyolefin skeleton through Pd(II) catalysis. *ACS Catal.* **2022**, *12*, 3430–3443.
129 Liu, Y.; Yang, G.; Li, C.; Tan, C.; Chen, M. Ligand pre-inserted α-diimine palladium catalysts and mechanism studies in olefin polymerization. *Polym. Chem.* **2023**, *15*, 40–45.
130 He, H.; Wang, W.; Pang, W.; Zou, C.; Peng, D. Double stimulus-responsive palladium catalysts for ethylene polymerization and copolymerization. *Chin. Chem. Lett.* **2024**, *35*, 109534.
131 Ji, H.; Zhang, Y.; Chi, Y.; Jian, Z. Concerted flexible and steric strategy in α-diimine nickel and palladium mediated insertion (co-)polymerization. *Polymer* **2024**, *290*, 126591.
132 Zhong, S.; Tan, Y.; Zhong, L.; Gao, J.; Liao, H.; Jiang, L.; Gao, H.; Wu, Q. Precision synthesis of ethylene and polar monomer copolymers by palladium-catalyzed living coordination copolymerization. *Macromolecules* **2017**, *50*, 5661–5669.
133 Zhong, L.; Zheng, H.; Du, C.; Du, W.; Liao, G.; Cheung, C. S.; Gao, H. Thermally robust α-diimine nickel and palladium catalysts with constrained space for ethylene (co)polymerizations. *J. Catal.* **2020**, *384*, 208–217.
134 Zheng, H.; Zhong, L.; Du, C.; Du, W.; Cheung, C. S.; Ruan, J.; Gao, H. Combining hydrogen bonding interactions with steric and electronic modifications for thermally robust α-diimine palladium catalysts toward ethylene (co)polymerization. *Catal. Sci. Technol.* **2021**, *11*, 124–135.
135 Guo, L.; Zhao, W.; Ji, M.; Chen, W.; Li, P.; Li, L.; Li, J.; Liu, Z. Dearomatized diimines for nickel(II) and palladium(II) catalyzed ethylene polymerization and copolymerization. *Inorg. Chem. Front.* **2024**, *11*, 1394–1412.
136 Dai, S.; Li, S.; Xu, G.; Wu, C.; Liao, Y.; Guo, L. Flexible cycloalkyl substituents in insertion polymerization with α-diimine nickel and palladium species. *Polym. Chem.* **2020**, *11*, 1393–1400.
137 Lu, Z.; Ge, Y.; Dai, S. Flexible axial shielding strategy for improving ethylene (co)polymerization with 8-cycloalkylnaphthyl a-diimine catalysts. *Inorg. Chem.* **2023**, *62*, 14888–14895.
138 Fan, H.; Kang, X.; Dai, S. Stable ultrahighly branched polyethylene synthesis *via* externally robust chain-walking polymerization. *ACS Catal.* **2024**, *14*, 13531–13541.
139 Dai, J.; Dai, S. Flexible α-diimine Ni(II) and Pd(II) catalysts featuring backbone and axial cycloalkyl substituents in ethylene (co)polymerization. *J. Polym. Sci.* **2025**, *63*, 1527–1535.
140 Wang, H.; Lu, Z.; Dai, S. Synthesis of hyperbranched polyethylene and carboxylate functionalized polyethylene using bis(benzocyclopentyl) α-diimine Pd(II) catalysts with axial substituent-constrained strategy. *Eur. Polym. J.* **2023**, *196*, 112247.
141 Ma, M.; Dai, S. Flexible monoarylmethyl substituents in an efficient synthesis of hyperbranched polyethylene and polar-functionalized polyethylene. *ACS Appl. Polym. Mater.* **2024**, *6*, 12781–12788.
142 Wu, X.; Zou, W.; Dai, S. Functionalized semi-crystalline polyethylene with polar groups at branch end enabled by bulky cationic palladium catalysts. *J. Polym. Sci.* **2023**, *61*, 3288–3294.
143 Lu, W.; Xu, G.; Chang, G.; Wang, H.; Dai, S. Synthesis of highly branched polyethylene and ethylene-MA copolymers using hybrid bulky α-diimine Pd(II) catalysts. *J. Organomet. Chem.* **2021**, *956*, 122118.
144 Lu, W.; Ding, B.; Dai, S. Control of chain transfer and chain walking by tailored metal–π interactions in polymerization catalysis. *J. Catal.* **2024**, *435*, 115550.
145 Lu, Z.; Ding, B.; Dai, S. Suppression of chain walking and chain transfer in ethylene (co)polymerization with iminodibenzyl substituents containing second coordination spheres. *Macromolecules* **2024**, *57*, 5262–5270.
146 Wang, Y.; Dai, S. Exploring the *o*-aryl halogen effects of α-diimine Pd(II) catalysts on ethylene (co)polymerization. *Catal. Sci. Technol.* **2025**, *15*, 2822–2828.
147 Dai, S.; Li, S. Effect of aryl orientation on olefin polymerization in iminopyridyl catalytic system. *Polymer* **2020**, *200*, 122607.
148 Li, S.; Dai, S. Highly efficient incorporation of polar comonomers in copolymerizations with ethylene using iminopyridyl palladium system. *J. Catal.* **2021**, *393*, 51–59.
149 Ge, Y.; Lu, Z.; Dai, S. Flexible axial shielding strategy for the synthesis of high-molecular-weight polyethylene and polar functionalized polyethylene with pyridine-imine Ni(II) and Pd(II) complexes. *Organometallics* **2022**, *41*, 2042–2049.
150 Yan, Z.; Bi, H.; Ding, B.; Wang, H.; Xu, G.; Dai, S. A rigid-flexible double-layer steric strategy for ethylene (co)oligomerization with pyridine-imine Ni(II) and Pd(II) complexes. *New J. Chem.* **2022**, *46*, 8669–8678.
151 Ding, B.; Chang, G.; Yan, Z.; Dai, S. Ethylene (co) oligomerization using iminopyridyl Ni(II) and Pd(II) complexes bearing benzocycloalkyl moieties to access hyperbranched ethylene oligomers and ethylene-MA co-oligomers. *Frontiers in Chemistry* **2022**, *10*, 961426.
152 Wu, X.; Xu, G.; Lu, W.; Li, Z.; Dai, S. Ethylene (co)oligomerization in alkane solvents facilitated by rigid-flexible double-layer steric strategy. *Eur. Polym. J.* **2022**, *177*, 111459.
153 Liao, Y.; Cai, Q.; Dai, S. Synthesis of high molecular weight polyethylene and e-MA copolymers using iminopyridine Ni(II) and Pd(II) complexes containing a flexible backbone and rigid axial substituents. *Chinese J. Polym. Sci.* **2023**, *41*, 233–239.
154 Ma, M.; Dai, S. Monoarylmethyl substituents dictate stability and chain transfer behavior in late transition metal pyridine-imine catalytic systems. *Organometallics* **2025**, *44*, 2219–2227.
155 Fan, H.; Ma, M.; Dai, S. Enhanced suppression of chain transfer in ethylene (co)polymerization *via* synergistic axial substituent effects in pyridine-imine Ni(II) and Pd(II) catalysts. *Polym. Chem.* **2025**, *16*, 4764–4773.
156 Li, S.; Lu, Z.; Fan, W.; Dai, S. Efficient incorporation of a polar comonomer for direct synthesis of hyperbranched polar functional ethylene oligomers. *New J. Chem.* **2021**, *45*, 4024–4031.
157 Fan, H.; Chang, G.; Bi, H.; Gui, X.; Wang, H.; Xu, G.; Dai, S. Facile synthesis of hyperbranched ethylene oligomers and ethylene/methyl acrylate co-oligomers with different microscopic chain architectures. *ACS Polymers Au* **2022**, *2*, 88–96.
158 Ge, Y.; Li, S.; Wang, H.; Dai, S. Synthesis of branched polyethylene and ethylene-MA copolymers using unsymmetrical iminopyridyl nickel and palladium complexes. *Organometallics* **2021**, *40*, 3033–3041.
159 Hu, H.; Zhang, L.; Gao, H.; Zhu, F.; Wu, Q. Design of thermally stable amine–imine nickel catalyst precursors for living polymerization of ethylene: Effect of ligand substituents on catalytic behavior and polymer properties. *Chem. Eur. J.* **2014**, *20*, 3225–3233.
160 Hu, H.; Gao, H.; Chen, D.; Li, G.; Tan, Y.; Liang, G.; Zhu, F.; Wu, Q. Ligand-directed regioselectivity in amine-imine nickel-catalyzed 1-hexene polymerization. *ACS Catal.* **2015**, *5*, 122–128.
161 Hu, H.; Chen, D.; Gao, H.; Zhong, L.; Wu, Q. Amine–imine palladium catalysts for living polymerization of ethylene and

copolymerization of ethylene with methyl acrylate: Incorporation of acrylate units into the main chain and branch end. *Polym. Chem.* **2016**, *7*, 529–537.
162 Liao, H.; Zhong, L.; Xiao, Z.; Zheng, T.; Gao, H.; Wu, Q. *α*-diamine nickel catalysts with nonplanar chelate rings for ethylene polymerization. *Chem. Eur. J.* **2016**, *22*, 14048-14055.
163 Zhong, L.; Li, G.; Liang, G.; Gao, H.; Wu, Q. Enhancing thermal stability and living fashion in *α*-diimine–nickel-catalyzed (co)polymerization of ethylene and polar monomer by increasing the steric bulk of ligand backbone. *Macromolecules* **2017**, *50*, 2675–2682.
164 Zheng, T.; Liao, H.; Gao, J.; Zhong, L.; Gao, H.; Wu, Q. Synthesis and characterization of *α*-diamine palladium complexes and insight into hybridization effects of nitrogen donor atoms on norbornene (co)polymerizations. *Polym. Chem.* **2018**, *9*, 3088–3097.
165 Zheng, H.; Pei, L.; Deng, H.; Gao, H.; Gao, H. Electronic effects of amine-imine nickel and palladium catalysts on ethylene (co)polymerization. *Eur. Polym. J.* **2023**, *184*, 111773.
166 Ding, L.; Cheng, H.; Li, Y.; Tanaka, R.; Shiono, T.; Cai, Z. Efficient ethylene copolymerization with polar monomers using palladium anilinonaphthoquinone catalysts. *Polym. Chem.* **2018**, *9*, 5476–5482.
167 Zhang, H.; Zou, C.; Zhao, H.; Cai, Z.; Chen, C. Hydrogen-bonding-induced heterogenization of nickel and palladium catalysts for copolymerization of ethylene with polar monomers. *Angew. Chem. Int. Ed.* **2021**, *60*, 17446–17451.
168 Zhang, H.; Zhang, Z.; Cai, Z.; Li, M.; Liu, Z. Influence of silica-supported alkylaluminum on heterogeneous zwitterionic anilinonaphthoquinone nickel and palladium-catalyzed ethylene polymerization and copolymerization with polar monomers. *ACS Catal.* **2022**, *12*, 9646–9654.
169 Guironnet, D.; Roesle, P.; Rünzi, T.; Göttker-Schnetmann, I.; Mecking, S. Insertion polymerization of acrylate. *J. Am. Chem. Soc.* **2009**, *131*, 422–423.
170 Neuwald, B.; Falivene, L.; Caporaso, L.; Cavallo, L.; Mecking, S. Exploring electronic and steric effects on the insertion and polymerization reactivity of phosphinesulfonato PdII catalysts. *Chem. Eur. J.* **2013**, *19*, 17773–17788.
171 Karimi, M.; Arabi, H.; Sadjadi, S. New advances in olefin homo and copolymerization using neutral, single component palladium/nickel complexes ligated by a phosphine-sulfonate. *J. Catal.* **2022**, *412*, 59–70.
172 Tan, C.; Qasim, M.; Pang, W.; Chen, C. Ligand-metal secondary interactions in phosphine-sulfonate palladium and nickel catalyzed ethylene (co)polymerization. *Polym. Chem.* **2020**, *11*, 411–416.
173 Xia, J.; Han, Y.; Kou, S.; Zhang, Y.; Jian, Z. Exploring steric effect of electron-donating group in palladium and nickel mediated ethylene polymerization and copolymerization with polar monomers. *Eur. Polym. J.* **2021**, *160*, 110781.
174 Li, Y.; Cao, G.; Cao, Y. Enhanced mechanical properties of acrylate and 5-vinyl-2-norbornene-based ethylene terpolymers: Rational design and synthesis using remotely modulated phosphine-sulfonate palladium complexes. *Polym. Chem.* **2024**, *15*, 4662–4672.
175 Wang, Z.; Liu, Y.; Pang, W.; Chen, A.; Chen, M. Polyolefin vitrimers bearing acetoacetate functionality. *Sci. China Chem.* **2024**, *67*, 3861–3867.
176 Ye, J.; Mu, H.; Wang, Z.; Jian, Z. Heteroaryl backbone strategy in bisphosphine monoxide palladium-catalyzed ethylene polymerization and copolymerization with polar monomers. *Organometallics* **2019**, *38*, 2990–2997.
177 Mu, H.; Ye, J.; Zhou, G.; Li, K.; Jian, Z. Ethylene polymerization and copolymerization with polar monomers by benzothiophene-bridged BPMO-Pd catalysts. *Chinese J. Polym. Sci.* **2020**, *38*, 579–586.
178 Zhou, G.; Mu, H.; Jian, Z. A comprehensive picture on catalyst structure construction in palladium catalyzed ethylene (co)polymerizations. *J. Catal.* **2020**, *383*, 215–220.
179 Li, K.; Ye, J.; Wang, Z.; Mu, H.; Jian, Z. Indole-bridged bisphosphine-monoxide palladium catalysts for ethylene polymerization and copolymerization with polar monomers. *Polym. Chem.* **2020**, *11*, 2740–2748.
180 Cai, Z.; Li, M.; Cao, L. Synthesis and characterization of phosphinobenzenamine palladium complexes and their application in ethylene polymerization and copolymerization with polar monomers. *Organometallics* **2022**, *41*, 3538–3545.
181 Nakano, R.; Nozaki, K. Copolymerization of propylene and polar monomers using Pd/IzQO catalysts. *J. Am. Chem. Soc.* **2015**, *137*, 10934–10937.
182 Akita, S.; Nozaki, K. Copolymerization of ethylene and methyl acrylate by palladium catalysts bearing IzQO ligands containing methoxyethyl ether moieties and salt effects for polymerization. *Polym. J.* **2021**, *53*, 1057–1060.
183 Hu, X.; Chen, J.; Li, Q.; Kang, X.; Jian, Z. A facile neutral nickel catalyst platform for high-temperature solution copolymerization of ethylene and acrylate. *Angew. Chem. Int. Ed.* **2026**, *65*, e25742.